Evaluating clouds, aerosols, and their interactions in three global climate models using satellite simulators and observations

George A. Ban-Weiss[1*], Ling Jin[2], Susanne E. Bauer[3], Ralf Bennartz[4,5], Xiaohong Liu[6,7], Kai Zhang[7], Yi Ming[8], Huan Guo[9], Jonathan H Jiang[10]

[1] Civil and Environmental Engineering, University of Southern California, Los Angeles, CA
[2] Lawrence Berkeley National Laboratory, Berkeley, CA
[3] NASA Goddard Institute for Space Studies and The Earth Institute at Columbia University, New York, NY
[4] Dept of Earth and Environmental Sciences, Vanderbilt University, Nashville, TN
[5] Atmospheric and Oceanic Sciences, University of Wisconsin, Madison, WI
[6] Department of Atmospheric Science, University of Wyoming, Laramie, WY
[7] Atmospheric Sciences & Global Change Division, Pacific Northwest National Laboratory, Richland, WA
[8] Geophysical Fluid Dynamics Laboratory, NOAA, Princeton, New Jersey
[9] UCAR Visiting Scientist Programs, Geophysical Fluid Dynamics Laboratory, NOAA, Princeton, New Jersey, USA.
[10] Jet Propulsion Laboratory, California Institute of Technology, Pasadena, California

* Corresponding Author:
George Ban-Weiss
email: banweiss@usc.edu
phone: +1 213 740 9124
Civil and Environmental Engineering
University of Southern California
Los Angeles, CA 90232

Accepted Article

This article has been accepted for publication and undergone full peer review but has not been through the copyediting, typesetting, pagination and proofreading process which may lead to differences between this version and the Version of Record. Please cite this article as doi: 10.1002/2014JD021722

©2014 American Geophysical Union. All rights reserved.

Abstract

Accurately representing aerosol-cloud interactions in global climate models is challenging. As parameterizations evolve, it is important to evaluate their performance with appropriate use of observations. In this investigation we compare aerosols, clouds, and their interactions in three global climate models (GFDL-AM3, NCAR-CAM5, GISS-ModelE2) to MODIS satellite observations. Modeled cloud properties are diagnosed using a MODIS simulator. Cloud droplet number concentrations (*N*) are computed identically from satellite-simulated and MODIS-observed values of liquid cloud optical depth and droplet effective radius. We find that aerosol optical depth (τ_a) simulated by models is similar to observations in many regions around the globe. For *N*, AM3 and CAM5 capture the observed spatial pattern of higher values in coastal marine stratocumulus versus remote ocean regions, though modeled values in general are higher than observed. Aerosol-cloud interactions were computed as the sensitivity of ln(*N*) to ln(τ_a) for coastal marine liquid clouds near South Africa (SAF) and Southeast Asia (SEA) where τ_a varies in time. AM3 and CAM5 are more sensitive than observations, while the sensitivity for ModelE2 is statistically insignificant. This widely used sensitivity could be subject to misinterpretation due to the confounding influence of meteorology on both aerosols and clouds. A simple framework for assessing the sensitivity of ln(*N*) to ln(τ_a) at constant meteorology illustrates that observed sensitivity can change from positive to statistically insignificant when including the confounding influence of relative humidity. Satellite-simulated versus standard model values of *N* from CAM5 are compared in SAF; standard model values are significantly lower with a bias of 83 cm^{-3}.

©2014 American Geophysical Union. All rights reserved.

Accepted Article

1 Introduction

Atmospheric aerosols affect Earth's energy balance and hydrological cycle. Aerosols absorb and scatter sunlight (aerosol direct effect), change the thermodynamic structure of the atmosphere (aerosol semi-direct effect), alter cloud microphysics (first indirect effect), and alter cloud macrophysics (second indirect effect) [e.g. *Ramanathan et al.*, 2001; *Menon* 2004; *Hansen et al.*, 2005; *Lohmann and Feichter*, 2005; *Ban-Weiss et al.*, 2012.; *IPCC* 2013]. The first aerosol indirect effect [*Twomey*, 1977] occurs when increases in concentrations of aerosols that serve as cloud condensation nuclei (CCN) lead to increases in cloud droplet number concentrations (N). For a given amount of cloud liquid water this would lead to smaller cloud droplets and higher cloud albedo. Quantitative assessment of this microphysical effect at global scale is challenging and aerosol indirect effects continue to be a major source of uncertainty in modeling the climate of Earth [*IPCC*, 2007; *IPCC*, 2013].

Feingold et al. [2001] proposed assessing the first aerosol indirect effect using an observable indicator ratio termed Aerosol Indirect Effect, AIE = $-\Delta\ln r_e/\Delta\ln \tau_a$, where r_e is the cloud droplet effective radius (defined as the ratio of third to the second moment of the cloud droplet size distribution) and τ_a is the aerosol optical depth. Alternative observable properties for clouds (e.g. cloud optical depth (τ_c) or N) and aerosols (e.g. aerosol number concentration or aerosol index) can be used with this approach [*McComiskey and Feingold*, 2012]. Cloud droplet effective radius and cloud optical depth have been frequently used in past studies as they are readily available from satellite observations. Note that use of these cloud properties to assess indirect effects requires constraining the cloud liquid water path in order to isolate changes in microphysics [*McComiskey et al.*, 2009]. In contrast, cloud droplet number

©2014 American Geophysical Union. All rights reserved.

Accepted Article

concentration N is decoupled from macrophysics [*Brenguier et al*., 2000] and therefore $\Delta\ln N/\Delta\ln \tau_a$ can be assessed without the need for constraining cloud liquid water. However, N is not a readily available satellite product and requires calculation using established algorithms [e.g. *Bennartz*, 2007]. As reviewed in *McComiskey and Feingold* [2012], a wide range of values for AIE have been reported in the past two decades using ground [e.g. *Feingold et al.*, 2003; *McComiskey et al.*, 2009; *Zhao et al*., 2012], airborne [e.g. *Ramanathan*, 2001; *Twohy et al*., 2005], and satellite-based [e.g. *Kaufman et al*., 2005; *Quaas et al*., 2006; *Jiang et al*., 2008] observations. Note that the liquid water constraint was not applied in most satellite studies, which may introduce variability in the reported AIE range. Quaas et al. [2006; 2009] represent an exception in that they computed N from satellite observations in their studies of AIE.

There are a number of challenges in quantifying aerosol indirect effects from observations. Ground and airborne measurements have used a variety of instruments with potentially different sensitivities and are often limited to certain geographic regions and time periods [*Rosenfeld and Feingold*, 2003]. Observations from satellite sensors reveal aerosol and cloud properties with more extensive temporal and spatial coverage, providing observations at the global scale [*Min et al*., 2012]. However, satellite retrievals of aerosol and cloud properties can contain artifacts. For example, (1) humidification can cause aerosols to swell near clouds and thus impact their optical properties [*Myhre et al*., 2007; *Quaas et al*., 2010; *Twohy et al*., 2009]; (2) radiation scattered by cloud edges may brighten the aerosol fields and cause contamination of aerosol optical depth [*Marshak et al*., 2006; 2008]; and (3) retrieval of cloud properties such as liquid water path and effective radius can be biased when variabilities in cloud adiabaticity and geometrical thickness are not adequately

©2014 American Geophysical Union. All rights reserved.

Accepted Article

accounted for [*Min et al*., 2012]. Quantification of aerosol indirect effects is also sensitive to the spatial scale at which data is aggregated [*Grandey and Stier*, 2010; *McComiskey and Feingold*, 2012]. It also varies by cloud regime [*Gryspeerdt and Stier*, 2012], showing the importance of computing statistics over areas with homogeneous cloud types.

Aerosol loadings and cloud properties are both dependent on meteorology at a range of spatial scales. For example, in near-coast subtropical marine environments, variability in synoptic and mesoscale meteorology can affect the magnitude or direction of winds, as well as properties of the marine boundary layer. This variability can directly impact the source and transport strength of aerosols. It can also impact the properties of the marine environment through, for example, changes in the temperature, relative humidity (RH), or stability of the air mass. In many case these meteorological shifts may directly contribute to changes in clouds even though aerosols are at the same time varying. This covariation in clouds, aerosols, and meteorology could potentially result in observed aerosol-cloud sensitivities that are not actually caused by aerosol-cloud interactions [e.g. *George and Wood*, 2010]. Some studies have indicated that meteorological versus aerosol associations with cloud properties are nearly orthogonal, suggesting that derived cloud-aerosol sensitivities are minimally confounded by meteorology [e.g. *Kaufman et al*., 2005; *Koren* et al., 2010]. Other studies found that meteorology played an important role in altering the apparent interactions of clouds and aerosols [e.g. *Engström and Ekman*, 2010; *George and Wood*, 2010; *Jiang et al*., 2011; *Petters et al*., 2013]. Note that these studies have largely focused on cloud macrophysical properties (e.g. cloud fraction and liquid water path) and not cloud microphysical properties. However,

©2014 American Geophysical Union. All rights reserved.

Accepted Article

aerosol and cloud microphysical properties can both be sensitive to certain meteorological variables. For example, the aforementioned changes in relative humidity of an air mass can alter τ_a via humidification of aerosols, a nonlinear process that is especially important at high RH in conditions favorable for cloud formation. There is also some evidence from observations that large-scale meteorology can modulate microphysical properties of marine stratocumulus clouds, but the extent to which this occurs cannot be quantified from observations alone [e.g. *Wood et al*., 2008; *George and Wood*, 2010]. Entrainment and mixing of (dry) environmental air into the cloud layer can affect clouds at different spatial scales, including the microphysical scale, since it can broaden the droplet size distribution. A previous modeling study [*Barahona et al.*, 2011, also see references therein] showed that entrainment can have an important impact on both N and r_e. The magnitude of the influence of entrainment is a strong function of the temperature differential between the cloudy and environmental air, as well as the relative humidity of the environmental air [*Barahona and Nenes*, 2007; *Ghan et al.*, 2011]. Other studies have shown that the modulating effects of entrainment on microphysical properties can largely obscure observations of the first aerosol indirect effect [*Kim et al.*, 2008]. While past studies often assess statistical relationships between aerosol and cloud properties at subseasonal scales to minimize the confounding effects of meteorology [e.g. *Quaas et al.*, 2009], even subseasonal variations can be important [*George and Wood*, 2010]. Further research is needed to understand possible confounding effects of meteorology on assessing the first aerosol indirect effect.

Global climate models now incorporate representations of aerosol indirect effects to help assess impacts of past and future changes in anthropogenic and natural aerosols

©2014 American Geophysical Union. All rights reserved.

Accepted Article

on cloud properties. As microphysical processes in clouds operate on much smaller scales than GCM grid cells, representing aerosol-cloud interactions involves parameterizations. Until recently such parameterizations have largely been based on empirical fits relating e.g. cloud droplet number concentration and aerosols using measured data [e.g. *Menon et al*., 2008]. Many GCMs now include more physically based schemes for at least some cloud regimes that represent the physics of aerosol activation including the influence of updraft velocity [*Abdul-Razzak and Ghan*, 2000; *Nenes and Seinfeld*, 2003; *Fountoukis and Nenes*, 2005; *Ming et al*., 2006; *Kumar et al*., 2009; and reviewed in *Ghan et al*., 2011 and *Barahona et al*., 2011]. The microphysics of cloud droplets can be modeled in GCMs using "bulk" schemes that assume a functional form for the cloud droplet size distribution. Bulk schemes vary by the number of moments represented. For example, one-moment schemes can predict cloud water mixing ratio while two-moment schemes can also predict N [e.g. *Morrison and Gettelman*, 2008]. Furthermore, aerosol schemes have evolved from simple mass based schemes to microphysical schemes that resolve the evolution of size distributions by calculating prognostic aerosol number concentrations. Evaluating new aerosol and cloud parameterizations as they are introduced into climate models is crucial for improving confidence in model predictions of aerosol indirect forcing. Satellite observations in general are uniquely suited for evaluating GCM simulations due to their spatial and temporal coverage [e.g. *Jiang et al.*, 2012]. In a recent study, *Quaas et al*. [2009] evaluated modeled aerosol-cloud interactions in 10 GCMs using satellite observations. They computed the previously discussed AIE metric applied to N, liquid water path, cloud fraction, cloud albedo, and more. This work demonstrated that statistical relationships of clouds and aerosols exhibited differences between GCMs and satellite observations. Besides the uncertainties associated with satellite

©2014 American Geophysical Union. All rights reserved.

Accepted Article

observations and model parameterizations mentioned previously, model-satellite differences could also be partly attributed to inherent differences in retrieved quantities viewed from space versus model variables [*Bodas-Salcedo et al*., 2011]. For example, retrievals derive geophysical parameters from radiances at particular wavelengths. Using satellite simulators to derive model variables in GCMs could help to minimize the comparison biases [*Kay et al*., 2012].

In this work, aerosols, clouds, and signatures of their interactions in three GCMs are compared to satellite observations. We focus on evaluating the first aerosol indirect effect quantified by $\Delta\ln N/\Delta\ln \tau_a$, which allows isolation of the microphysical component of the AIE without the need for constraining the location and time dependent liquid water path. ($\Delta\ln N/\Delta\ln \tau_a$ is sometimes referred to as a "sensitivity" in this paper.) The CFMIP Observation Simulator Package (COSP) [*Bodas-Salcedo et al*., 2011] is used to produce GCM diagnostics that enhance comparability to observations. Cloud droplet number concentration N is computed for both satellite observations and satellite-simulated GCM values in a consistent way using an algorithm presented in *Bennartz* [2007]. Our analysis of aerosol-cloud interactions is focused on near-coast marine areas near South Africa (SAF) and South East Asia (SEA), which have persistent stratocumulus clouds and are subject to aerosol pollution from near-by land regions [e.g. *Bennartz*, 2007; *Rausch et al*., 2010]. We present a simple statistical framework for evaluating how the influence of meteorology on N and τ_a can confound interpretation of the AIE metric (e.g. $\Delta\ln N/\Delta\ln\tau_a$). Lastly, we compare satellite-simulated versus standard model values of N.

©2014 American Geophysical Union. All rights reserved.

2 Methods

Aerosols, clouds, and signatures of aerosol-cloud interactions were investigated in GCMs and satellite observations. Three GCMs were included: 1) National Center for Atmospheric Research (NCAR) Community Atmosphere Model 5 (CAM5) [*Neale et al*., 2010]; 2) Geophysical Fluid Dynamics Laboratory (GFDL) AM3 [*Donner et al*., 2011]; and 3) National Aeronautics and Space Administration (NASA) Goddard Institute for Space Studies (GISS) ModelE2 [*Schmidt et al*., 2014]. All three models were configured consistently with simulations submitted for the 5th Assessment Report (AR5) of the Intergovernmental Panel on Climate Change (IPCC) with the following two exceptions. In this study, ModelE2 simulated aerosols using a microphysical scheme called the Multiconfiguration Aerosol TRacker of mIXing state a.k.a. MATRIX [*Bauer et al*., 2008]. Also, adjustments to the cloud scheme in ModelE2 were made as described in *Kim et al*. [2012]. Observations were from the MODerate resolution Imaging Spectroradiometer (MODIS) on the Aqua satellite.

Differences in GCM-simulated versus satellite-observed aerosols and clouds can stem from many factors including 1) deficiencies in model parameterizations specific to aerosol and cloud physical processes, 2) the fact that satellite sensors and GCMs view the atmosphere in inherently different ways [*Bodas-Salcedo et al*., 2011; *Kay et al*., 2012], and 3) differences in observed versus modeled meteorology. In this study we seek to highlight differences in observations versus models due to deficiencies in parameterizations while minimizing differences due to (2) and (3). To achieve this goal we, a) use a satellite simulator that views modeled clouds as would a satellite sensor, b) extract model-simulated values at satellite observation overpass times, and c) nudge modeled winds to meteorological observations. In this way, differences

©2014 American Geophysical Union. All rights reserved.

Accepted Article

between models versus observations and also among the three models are largely caused by parameterizations directly related to aerosol and cloud processes. More details are listed below.

For both observations and models the period of analysis is January 1, 2007 to January 1, 2009. This period was chosen as observations from both MODIS and CALIPSO (to be reported in a future paper) are available. Simulations were limited to two years because of the large data storage needs required by saving 3-dimensional output at high time resolution (see Section 2.2). In this work we focus on aerosols and clouds in two maritime regions: South Africa (SAF) and Southeast Asia (SEA). SAF was defined as 25°S – 5°S, 0° – 15°E, and SEA was 15°N – 35°N, 120°E – 140°E (see Figure 1 for region outlines). These regions were selected due to their prevalence of marine boundary layer clouds and variations in aerosol loading from advection of aerosols generated mostly by biomass burning (SAF, SEA) and combustion of fossil fuel (SEA). The boundaries of these regions are similar to those used by other studies of satellite observed cloud microphysical parameters in maritime stratocumulus areas [*Rausch et al*., 2010; *Fu et al.*, 2014]. However, in our study the boundaries were somewhat smaller than used in *Rausch et al*. to ensure aerosol and cloud properties were mostly homogeneous within the regions.

2.1 Details on Observations

Satellite observations were from the MODIS sensor onboard Aqua, a sun-synchronous satellite that crosses the equator at 01:30 and 13:30 h (local time). In this study data from 13:30 h were used. MODIS senses 36 spectral bands with wavelengths ranging from 0.4 to 14.4 µm; spatial resolution varies by band from 250

©2014 American Geophysical Union. All rights reserved.

Accepted Article

– 1000 m. The sensor was launched on Aqua in 2002. In this work we use daily observations from Level 3 Collection 5 (L3C5) [*Remer et al*., 2005]. Datasets used include aerosol optical depth (τ_a), liquid cloud optical depth (τ_c), and liquid cloud droplet effective radius (r_e), all of which are at 1° x 1° spatial resolution. The accuracies of MODIS aerosol and cloud optical depth measurements are about 0.05 over the ocean and 0.15 over the land [*Remer et al*., 2005]. For cloud droplet effective radius, the typical MODIS uncertainty is ~10%, but can be larger depending on the corresponding cloud optical thickness, vertical homogeneity, and solar/viewing geometry [*Platnick et al*., 2003; *Nakajima et al*., 2010; *Zhang and Platnick*, 2011]. *Zhang and Platnick* found that r_e computed using three different MODIS bands was consistent to within ±2 μm for spatially homogeneous coastal stratocumulus, which is the cloud regime of focus for this study. (Large differences sometimes greater than 10 μm were found for trade wind cumulus regimes.) Bréon and Doutriaux-Boucher (2005) compared r_e from MODIS to that independently derived from another satellite sensor, Polarization and Directionality of the Earth's Reflectances (POLDER). MODIS was consistently higher than POLDER by about 2 μm over remote ocean regions, though the two were highly correlated. Lower correlation was observed when POLDER-derived r_e was < 7 μm, most common over land and in polluted ocean regions. The accuracies/uncertainties for MODIS described here are based on validation statistics of large amounts of data. Each individual/instantaneous satellite measurement has higher uncertainty.

It is important to note that cloud properties observed by MODIS are in-cloud values, which is also how they are reported in this paper. The cloud microphysical quantity of focus is cloud droplet number concentration (*N*), which is calculated using τ_c and r_e,

©2014 American Geophysical Union. All rights reserved.

Accepted Article

as explained in section 2.3. MODIS observed liquid cloud fraction used for screening (see Section 2.3.2) cloud variables refers to the fraction of valid liquid retrievals in 1° x 1° degree grid boxes for Level 3 observations. MODIS-simulated liquid cloud fraction is also used for screening model results for clouds.

Meteorological observations used were the ERA-Interim reanalysis from the European Centre for Medium-Range Weather Forecasts (ECMWF). 6-hourly values were used to extract values in SAF and SEA at the time nearest the Aqua overpass time of 13:30 h local.

2.2 Details on Global Climate Models

Simulations using NCAR CAM5 version 5.1 (1.9° x 2.5° latitude x longitude), GFDL AM3 (2° x 2.5°), and GISS ModelE2 (2° x 2.5°) were carried out using prescribed sea surface temperatures (SSTs). CMIP5 emissions [*Lamarque et al*., 2010] were used for all models. Natural aerosol emissions are not specified in CMIP5 and therefore could include model dependency. In all three models, dust and sea salt aerosol emissions are calculated interactively. In ModelE2, the emissions of sea salt and mineral dust depend on surface wind speed and other surface conditions [*Bauer et al*., 2008]. In AM3, dust emissions depend on wind speeds at 10 m, accumulated sediments at the topographic depression regions, particle size, and surface wetness, following the parameterization by *Ginoux et al*. [2001]. Sea salt emissions from the ocean also highly depend on the wind speeds at 10 m [*Monahan et al*., 1986]. In CAM5, dust emissions are dependent on 10 m wind speed, vegetation cover, and soil properties (preferential area and soil wetness). Sea salt emissions are dependent on 10 m wind speed and SSTs [*Liu et al*., 2012].

©2014 American Geophysical Union. All rights reserved.

Accepted Article

Modeled horizontal winds (u- and v-components) were nudged to reanalysis data as follows. In ModelE2 the horizontal wind components were nudged toward the NCEP reanalysis data, which are available every 6 hours and are linearly interpolated to the model 30-minute time step. In AM3, horizontal winds were nudged towards the T62 NCEP reanalysis data set with a horizontal resolution of about 210 km [*Kalnay et al*., 1996]. The nudging relaxation timescale was six hours [see e.g. *Li et al.*, 2008]. In CAM5 horizontal winds were nudged toward the ERA-Interim reanalysis data set with a relaxation time scale of six hours. (Temperatures were also nudged in CAM5 using the same observational dataset and relaxation time.)

In all three climate models, SSTs and sea ice were prescribed using the Hadley Centre Sea Ice and Sea Surface Temperature data set [*Rayner et al*., 2003], following Atmospheric Model Intercomparison Project (AMIP) [*Gates*, 1992; *Gates et al*., 1999].

Table 1 summarizes and compares details on aerosol and cloud microphysical parameterizations for the three GCMs. Details for each model are as follows.

CAM5 used the Modal Aerosol Module (MAM3) representing three lognormal aerosol modes: Aitken, Accumulation, and Coarse [*Liu et al*., 2012]. The three aerosol modes represent multiple species: sulfate, black carbon, primary organic matter, secondary organic matter, soil dust, and sea salt. Ammonium is assumed to be associated with sulfate in the form of ammonium bisulfate. Both total particle number and mass mixing ratios of each mode are predicted. Cloud activation follows *Abdul*

©2014 American Geophysical Union. All rights reserved.

Accepted Article

Razzak and Ghan [2000] for stratiform clouds. Ice and mixed phase cloud microphysics is based on *Liu et al*. [2007] and *Gettelman et al*. [2010]. The *Morrison and Gettelman* [2008] and *Gettelman et al*. [2008] double moment microphysics for stratiform clouds is used. Aerosol water uptake is based on the Köhler theory [e.g. *Pruppacher and Klett*, 1997] for multiple external lognormal modes that are composed of internally mixed soluble and insoluble material. Both the first and second indirect effects are considered. (Cloud macrophysics is based on *Park et al.* [submitted].)

ModelE2 uses the MATRIX [*Bauer et al*., 2008], an aerosol microphysical scheme based on the quadrature method of moments. The mixing state of 16 aerosol populations is tracked including the following chemical species: sulfate, nitrate, black carbon, organic aerosols, sea salt and dust. To simulate the first indirect effect, a treatment similar to that described by *Menon et al*. [2010] is used, which includes several changes to the treatment of cloud drop and ice crystal nucleation following the scheme from *Morrison and Gettelman* [2008]. For cloud droplets, a prognostic equation to calculate cloud droplet number concentration is used, based on a simplified version of *Morrison and Gettelman* [2008] (Table 1). The source term of cloud droplets is obtained from MATRIX using the scheme of *Abdul-Razzak and Ghan* [2000]. The loss terms for cloud droplets include autoconversion, contact nucleation, and immersion freezing. Autoconversion is modeled as in *Del Genio* et al. [1996] (also see *Menon et al.*, [2008]) and is a function of cloud water content but not *N* or aerosol. As such, only the first aerosol indirect effect is included in the simulations. ModelE2 is described in [*Schmidt et al.*, 2014] and includes updated

©2014 American Geophysical Union. All rights reserved.

Accepted Article

turbulence [*Yao and Cheng*, 2012] and moist convection [*Del Genio et al.*, 2012] parameterizations.

AM3 predicts mass distributions of major aerosol components from emissions, including sulfate, black carbon, organic carbon, secondary organic aerosols, dust, and sea salt
[*Donner et al*., 2011]. Aerosol activation into liquid droplets follows a mechanistic scheme developed by *Ming et al*. [2006], depending on updrafts and aerosol characteristics and concentrations. Aerosol wet deposition is also coupled to cloud microphysics [*Giorgi and Chameides*, 1985; *Li et al*., 2008]. The AM3 cloud microphysical parameterization is a one-moment scheme except for cloud water. It follows *Rotstayn* [1997] with updated treatment of mixed-phase stratiform clouds [*Rotstayn et al*., 2000] and also includes some important changes as discussed in GFDL *Global Atmosphere Model Development Team* [2004]. The inclusion of cloud droplet activation by aerosols enables simulations of droplet sizes and allows for interactions between aerosols and clouds [*Ming et al.*, 2006, 2007; *Golaz et al*., 2011].

Cloud properties were calculated online using a satellite simulator called the CFMIP Observations Simulator Package (COSP) [*Bodas-Salcedo et al*., 2011]. While COSP has the capability to simulate many different satellite sensors, we focus on MODIS-simulated values in this investigation. To match the observations we extracted satellite-simulated liquid cloud optical depth τ_c and liquid cloud droplet effective radius r_e. We refer to results derived with COSP as “satellite-simulated” or “MODIS-simulated”.

©2014 American Geophysical Union. All rights reserved.

Accepted Article

Key aerosol, cloud, and meteorological variables of interest were output and saved every three hours (0, 3, 6, 9, 12, 15, 18, 21 GMT) for the entire two-year period. Values were instantaneous and not three-hour averages. This allowed for extraction of satellite-simulated model values in SAF and SEA at times nearest the Aqua satellite overpass times; actual model times extracted were 1200 h and 0300 h GMT for SAF and SEA, respectively, corresponding to noon local time. These daily "snapshots" of model values in each region were used for the analysis presented in this paper.

Calculation of cloud droplet number concentration (*N*)

N was calculated from satellite-observed and satellite-simulated GCM values of liquid r_e and τ_c using an algorithm that assumes clouds are adiabatically stratified [e.g. *Bennartz* 2007; *Rausch et al*., 2010]. This algorithm is now briefly described. A more in depth explanation can be found in *Bennartz* [2007] and *Rausch et al*. [2010].

2.3.1 Cloud macrophysics

The "activation" of aerosols into cloud droplets can be described as follows. Air parcels that ascend experience cooling due to adiabatic expansion. Once the water vapor in the cooling air parcel becomes saturated, aerosols of certain sizes and compositions that can serve as cloud condensation nuclei (CCN) begin accruing condensed water, initiating the base of a cloud. As droplets continue to ascend with the air parcel they follow the moist adiabatic lapse rate and continue to accrue condensed water. The rate of condensation is a function of excess water vapor and therefore parcel temperature. Since marine boundary layer clouds are relatively thin, they experience relatively little temperature fluctuation and therefore condensation

©2014 American Geophysical Union. All rights reserved.

Accepted Article

rate can be assumed constant. The liquid water content of maritime boundary layer clouds can therefore be expressed as

$$w(h) = c_w h \tag{1}$$

where $w(h)$ is the liquid water content (kg/m^3), c_w is the adiabatic condensation rate (kg/m^4), and h is the height above cloud base (m). There is observational evidence confirming the abiabaticity of maritime boundary layer clouds [e.g. *Duynkerke et al*. 1995; *Pawlowska and Brenguier*, 2000]. *In situ* observations also indicate that w near cloud top is about 80% the value suggested by strict adiabaticity (see *Rausch et al*. [2010] and references therein). We therefore assume c_w is 80% the adiabatic value (~0.8*2×10^{-6} kg m^{-4} = 1.6×10^{-6} kg m^{-4} for representative boundary layer temperatures). Entrainment of dry air, which can occur especially at the cloud top, is not included in this model. Inclusion of entrainment would tend to decrease w at the cloud top.

The liquid water path, W (kg/m^2), can be calculated by integrating $w(h)$ from the base to top of the cloud,

$$W = \frac{1}{2} c_w H^2 \tag{2}$$

where H is the cloud geometrical thickness (m).

2.3.2 Cloud microphysics

Cloud microphysics can be described by r_e and N. N can vary from ~25 cm^{-3} in pristine marine locations to over 100 or even 1000 cm^{-3} in polluted environments with high concentrations of CCN. However, observations have shown that values of N within a given boundary layer cloud are nearly constant [e.g *Pawlowska and*

©2014 American Geophysical Union. All rights reserved.

Accepted Article

Brenguier, 2000]. Thus, as *h* increases, cloud droplets grow as vapor condenses onto a fixed number of N. With this in mind, *W* can be expressed as

$$W = \frac{5}{9}\rho_{\mathrm{L}} r_{\mathrm{e}} \tau_{\mathrm{c}} \tag{3}$$

where ρ_{L} is the density of liquid water. The cloud optical thickness τ_{c} can then be related to N and *H* as

$$\tau_{\mathrm{c}} = \frac{3}{5}\pi Q \left[\frac{3c_{\mathrm{w}}}{4\pi\rho_{\mathrm{L}}}\right]^{2/3} [k(N)]^{1/3} H^{5/3} \tag{4}$$

$Q \approx 2$ is the scattering efficiency and $k \approx 0.8$ is the ratio between the volume mean radius and the effective radius.

Combining Eqns. (2) and (4) leads to

$$N = \frac{2^{-5/2}}{k} \tau_{\mathrm{c}}^{3} [W]^{-5/2} \left[\frac{3}{5}\pi Q\right]^{-3} \left[\frac{3}{4\pi\rho_{\mathrm{L}}}\right]^{-2} c_{\mathrm{w}}^{1/2} \tag{5}$$

Thus, N is derived from two independent observations, *W* and τ_{c}. It is important to note that in this formulation, *W* is the in-cloud liquid water path as observed by MODIS, not the grid cell average value. Values for *k*, *Q*, and c_w are as already discussed; the impact of uncertainty in these values is described in *Bennartz* [2007].

Assuming the cloud is adiabatically stratified, its macro- and microphysical properties can be fully described using any two of the following: retrieved quantities τ_{c} and r_{e}, and computed quantities *N*, *W*, and *H*. In this study our focus is on the microphysical

©2014 American Geophysical Union. All rights reserved.

Accepted Article

quantity *N*. Using the functional form of N as a function of τ_c and *W* as in equation (5), $N \propto \tau_c^{\,3} W^{-5/2}$. Alternatively, combining Eqns. (3) and (5) shows $N \propto \tau_c^{\,1/2}\, r_e^{\,-5/2}$.

Eq. (5) (and Eq. (3) for computing *W* from τ_c) was applied to each grid cell using both satellite observations and satellite-simulated GCM values. Note that instantaneous values for liquid clouds reported by COSP in AM3 and CAM5 are by default multiplied by C_F = liquid cloud fraction (i.e. at each model timestep the model reports $\tau_c \times C_F$ and $r_e \times C_F$). (These products are then used to calculate monthly mean cloud properties weighted by cloud fraction, which are not used in this investigation.) Since we require in-cloud values for computing *N*, we divided instantaneous model reported values by liquid cloud fraction to compute instantaneous in-cloud values for τ_c and r_e. To ensure the existence of large-scale clouds and reduce noise in the retrieval algorithms (see for example sources of error for r_e explained in section 2.1), we mask cloud variables at each time step for grid cells with liquid cloud fraction < 30%. Results are insensitive to the exact value of cloud fraction chosen for screening [*Bennartz*, 2007].

3 Results

3.1 Global maps

SAF and SEA are the focus of this study, but we first discuss these regions in the context of global distributions. Aerosol optical depths and cloud droplet number concentrations are emphasized but liquid cloud optical depths and droplet effective radii are also shown as they are used to calculate *N* using Eq. (5) and (3). All modeled cloud values reported here are computed using the COSP simulator for MODIS.

©2014 American Geophysical Union. All rights reserved.

Accepted Article

Maps of aerosol optical depth τ_a from MODIS observations and the three climate models are shown in Figure 1. Values are means over the entire analysis period (January 1 2007 – January 1 2009). Models capture many of the spatial patterns of τ_a observed by MODIS including local maxima in South America and central Africa from biomass burning, northern African from dust storms, and Southeast Asia from combustion of fossil fuels and biomass. Models also capture higher values in the eastern continental United States while high τ_a observed in the western United States is not simulated by the models. In the South American biomass burning region, values of τ_a for AM3 are similar in magnitude to the observations while values for CAM5 and ModelE2 are lower than observed. In the central African burning region, model values are similar to observations but the location with maximum τ_a varies by model. High values of τ_a observed over Northern Africa and the northern Atlantic Ocean are well captured by all three models. (The presence of the high albedo desert surface precludes the calculation of τ_a from observations in parts of Northern Africa, shown in black.) Models are similar to observations over the east Asian continent, though values appear lower than observed for CAM5. ModelE2 predicts higher τ_a in the Southern Oceans than observations while AM3 and CAM5 are lower than observed. Note that values for τ_a shown here are from standard model output and are not satellite simulated. However, we compared "all-sky" versus "clear-sky" τ_a in ModelE2 and found negligible differences. Clear-sky τ_a is more similar to observations since MODIS retrieves aerosol properties only in cloud-free pixels.

Accepted Article

©2014 American Geophysical Union. All rights reserved.

Maps of (in-cloud) liquid cloud optical depth from observations and satellite-simulated GCM results are shown in Figure 2. Two-year means for both MODIS observations and simulations are weighted by observed and satellite-simulated liquid cloud fraction, respectively. The weighting was performed for consistency with techniques used for MODIS monthly products (not used here), in which time averages for Level 3 products are weighted by the number of observations within each 1° x 1° degree grid box [*Pincus et al*., 2012]. (Note, however, that MODIS monthly products do not use the cloud fraction screening used in this investigation.) Spatial patterns over ocean regions are reasonably well captured by models including local maxima in the high latitudes and equatorial Pacific. Absolute values from all three models are generally higher than observations, especially for CAM5 and ModelE2. Land values are similar for observations versus AM3 and ModelE2, but values simulated by CAM5 are much higher than observations. Note that the in-cloud values of liquid τ_c presented in Figure 2 are not representative of grid-cell values. Though radiative transfer in the model atmosphere is ultimately calculated with grid cell values, in-cloud τ_c is more relevant to the microphysical effects of aerosols on clouds and is used to calculate *N* using Eq. (5) and (3). The fact that modeled τ_c is higher than observations is qualitatively consistent with *Kay et al.* [2012], who describe the well established compensating bias in global climate models of underestimating total cloud amount and overestimating cloud optical depth. While this bias was shown to be markedly improved in CAM5 versus an older version of CAM (version 4), both versions show total cloud amounts that are lower than observations. Underestimates were especially significant for subtropical marine boundary layer clouds due to the incorrectly simulated transition from stratocumulus- to cumulus-topped boundary layers.

©2014 American Geophysical Union. All rights reserved.

Accepted Article

Maps of liquid cloud droplet effective radius r_e from observations and satellite-simulated GCM results are shown in Figure 3. Two-year means are weighted by liquid cloud fraction as in Figure 2. Model values are lower than observations for most areas around the globe. Observed values over remote ocean regions are generally about 6 μm higher than simulated by models. There are especially large discrepancies in the Intertropical Convergence Zone (ITCZ). As expected, observed r_e is lower in coastal marine stratocumulus areas (e.g. SAF, SEA, and off the west coasts of South America) than remote ocean regions. These coastal environments experience higher concentrations of aerosols due to their close proximity to continental pollution. The higher concentrations of these aerosols that act as CCN lead to lower r_e. Both AM3 and CAM5 predict lower r_e in SAF than remote ocean regions, while in ModelE2 this pattern is reversed. The comparison of MODIS observations to AM3 is consistent with results reported in *Donner et al*. [2011].

Maps of cloud droplet number concentration *N* are shown in Figure 4. Values are means over the entire analysis period and are computed using Eq. (5) from MODIS observations and MODIS-simulated GCM results. The land is masked as in *Bennartz* [2007] because the adiabatic assumption used for deriving *N* is expected to be less valid here than over ocean regions [*Kim et al.*, 2005; *Gryspeerdt and Stier*, 2012]. (For reference, unmasked versions are in the Auxiliary Material.) The observations show low values of N on the order of 20-40 cm^{-3} in remote marine regions. N is higher in coastal marine environments that experience higher aerosol concentrations that act as CCN (e.g. SAF, SEA, and off the west coasts of North and South America), consistent with previously reported values that use this algorithm [*Bennartz*, 2007,

©2014 American Geophysical Union. All rights reserved.

Accepted Article

Rausch et al., 2010]. Both AM3 and CAM5 predict the expected spatial pattern of higher N in these near-coast marine regions versus remote ocean regions. This spatial pattern is predicted by ModelE2 in SEA but not off the west coasts of South Africa (SAF) and North and South America. (ModelE2 does however simulate a small area within SAF with higher *N*.) Differences between observed versus modeled N are caused by discrepancies in satellite observed versus simulated τ_c and r_e (Figure 2 and Figure 3). For example, higher predicted versus observed N for CAM5 in SAF and SEA are mostly due to the low simulated values for r_e.

3.2 Regional-mean time series

For the remainder of the analysis we focus on two coastal maritime regions that are influenced by variable aerosol loadings. The South African (SAF) region is influenced predominantly by biomass burning aerosols while the Southeast Asian (SEA) region is influenced by combustion of both fossil fuel and biomass. As before, all modeled cloud values reported here are computed using the COSP simulator for MODIS. Figure 5 shows regional-mean time series of dailies for these two regions, and Table 2 has the two-year means and standard deviations for these time series. We investigate these time series in detail because they are the basis for computing aerosol-cloud sensitivities presented in Section 3.3. We suggest that investigating the individual time series is an important first step before evaluating interactions among the variables to avoid misinterpretations by compensating errors.

SAF

First we assess unscreened liquid cloud fractions. Unlike all other cloud variables reported in this paper, these unscreened values include all grid cells within SAF rather than masking those with liquid cloud fraction < 30%. Unscreened liquid cloud fractions simulated by AM3 and CAM5 match the observations relatively well.

©2014 American Geophysical Union. All rights reserved.

Accepted Article

CAM5 captures the observed seasonal cycle while AM3 predicts the maximum liquid cloud fraction a couple months early each year. ModelE2 underestimates liquid cloud fraction and the seasonal cycle is out of phase, indicating that the model is still struggling to create stratocumulus clouds, as has been noted for previous versions [*Schmidt et al.*, 2006]. We note that modeling stratocumulus clouds has historically been a challenge for GCMs [e.g. *Zhang et al*, 2005; *Schmidt et al.*, 2006; *Donner et al.*, 2011; *Voldoire et al.* 2012, *Guo et al.*, 2014].

It is also useful to assess screened liquid cloud fraction where only grid cells with liquid cloud fraction ≥ 30% are included in the daily spatial means. AM3 and CAM5 values are near observations, while ModelE2 values are below observations between June and December. Screened liquid cloud fraction simulated by ModelE2 is nearer to observations than unscreened values. Missing data in the time series for ModelE2 indicates that there were no grid cells in SAF with liquid cloud fraction ≥ 30% for that day.

Simulated values for liquid cloud optical depth τ_c are near observations for AM3 and CAM5 for most of the year, whereas values for ModelE2 are higher than observed.

Observations of liquid cloud droplet effective radius r_e show a seasonal cycle with minimum values during JJA. Values simulated by CAM5 and AM3 are consistently below observations, while ModelE2 is consistently above observed values.

For completeness we include an assessment of cloud geometrical thickness *H* even though macrophysical cloud properties are not the focus of this study. Observations

©2014 American Geophysical Union. All rights reserved.

Accepted Article

indicate a two-year mean cloud thicknesses of 245 m with minimal seasonal cycle. Values for CAM5 are near observations, while AM3 values are lower and have a slightly more apparent seasonal cycle. Clouds in this region modeled by ModelE2 are thicker than observations.

Compared to observations, values for simulated *N* are much higher for CAM5 and somewhat higher for AM3. Values for ModelE2 are nearly the same as observations during the portions of the year that the model produces liquid clouds in this region. Observations identify a seasonal cycle with maximum *N* in JJA. CAM5 and AM3 reproduce this seasonal cycle. ModelE2 has missing values for most of JJA indicating that liquid cloud fraction was < 30%.

MODIS observations show a strong seasonal cycle for aerosol optical depth τ_a with maximum values up to around 1 in July, August, and September when biomass burning is prevalent. Modeled values of τ_a are near observations for most of the year though are underestimated during the burning season. AM3 also shows a spurious increase in τ_a during February and March. Two-year means for all models are below observations.

SEA

In SEA, both unscreened and screened liquid cloud fraction is remarkably well modeled by all three GCMs both in terms of absolute values and seasonal cycle (Figure 5b and Table 2). τ_c is also pretty well simulated by all three models. AM3 is near observations while CAM5 and Model2 are somewhat higher than observed. The amplitude of the annual cycle simulated by AM3 (CAM5) is slightly smaller (larger) than observed.

©2014 American Geophysical Union. All rights reserved.

Accepted Article

Simulated values of r_e are generally lower than observed for all three models. AM3 and ModelE2 are near observations during DJF and MAM, but below observations during the other seasons. Values of r_e for CAM5 are well below observations during the entire period with the two-year mean 6 μm below observations.

Observed cloud thickness *H* varies between about 300 and 500 m throughout the period. There is a stronger seasonal cycle in SEA than in SAF, with maximum thicknesses in SEA occurring during winters and minimum thicknesses during summers. Simulated values of *H* are near observations for all three models, though summertime values are lower than observations for CAM5 and AM3.

Observed cloud droplet number concentration *N* varies from about 50 to 200 μm throughout the period. Values of *N* during January through May are higher than the remainder of the year. CAM5 captures this seasonal cycle though with a much larger range in values of *N*. The seasonal cycles simulated by AM3 and ModelE2 are out of phase from observations. Simulated values for all three models are generally higher than observations for much of the analysis period. CAM5 simulates higher values of N for the entire period, while AM3 and ModelE2 are near observations during DJF and MAM but higher than observations during JJA and SON. Two-year means of *N* for all three models are higher than observations.

Observed τ_a ranges from about 0.1 to above 0.6 throughout the period. The seasonal cycle shows highest values during MAM. Simulated values from CAM5 are generally lower in magnitude with maxima occurring slightly earlier in the year than

©2014 American Geophysical Union. All rights reserved.

Accepted Article

observations. AM3 well predicts τ_a values but with seasonal maxima lagging observations by several months. The two-year mean for ModelE2 is higher than observations with seasonal maxima leading observations by several months.

3.3 Total sensitivity of *N* to aerosol

The variation in daily τ_a and N in SAF and SEA allow for assessing the sensitivity of N to τ_a. As has been used in past studies [e.g. *Quaas et al*., 2006, 2009], we use $\Delta\ln N/\Delta\ln\tau_a$ as a signature of interactions between cloud microphysics and aerosols. $\Delta\ln N/\Delta\ln\tau_a$ was computed using the daily time series shown in Figure 5, and the log sensitivity is used following *Feingold et al*. [2001]. Uncertainty estimates are calculated as 95% confidence intervals using daily values in the time series. Generally, positive sensitivities indicate that N increases with τ_a, an indicator of the first aerosol indirect effect. We note at this point that there may be limitations to this metric, which are further discussed in Section 3.4.

Figure 6a shows $\Delta\ln N/\Delta\ln\tau_a$ in SAF during the entire analysis period and separately for each season (see the Auxiliary Material for numerical values and the number of daily samples used to compute each sensitivity). For the entire period ("ALL" in Figure 6), the sensitivity calculated using observations is positive, indicating that N increases with τ_a. This sensitivity calculated using satellite-simulated AM3 results is statistically indistinguishable from the observations. CAM5 has higher sensitivity than observations, while ModelE2 has a lower sensitivity that is statistically indistinguishable from zero. Since the time series are not deseasonalized, it is likely that the sensitivities in "ALL" include co-variation in N and τ_a that are not causal. For this region, JJA provides the most statistically robust seasonal result because 1) τ_a

©2014 American Geophysical Union. All rights reserved.

Accepted Article

widely varies, and 2) a higher fraction of grid cells have liquid cloud fraction ≥ 30% and therefore each spatial mean is calculated using more data points (see the Auxiliary Material). $\Delta\ln N/\Delta\ln\tau_a$ during JJA calculated using AM3 model values shows higher sensitivity than observations. The sensitivity of CAM5 is also higher than observations but the two are not statistically distinguishable. $\Delta\ln N/\Delta\ln\tau_a$ in this region for ModelE2 has large error bars due to the relatively low number of days containing grid cells with liquid cloud fraction ≥ 30%.

$\Delta\ln N/\Delta\ln\tau_a$ for SEA is shown in Figure 6b. For the entire analysis period, fractional differences between observed and modeled sensitivities are similar in SEA and SAF. Absolute sensitivities are roughly two times larger in SEA versus SAF. This higher sensitivity in SEA can be qualitatively observed in the time series (Figure 5); annual cycles of τ_a have lower amplitude in SEA versus SAF, while for N the annual cycles are of similar amplitude in each region. Seasonal sensitivities calculated using observations are indistinguishable from zero. For SON and JJA, the model derived $\Delta\ln N/\Delta\ln\tau_a$ for AM3 and CAM5 are positive and statistically significant, while ModelE2 is negative and significant. We caution that discrepancies in seasonal sensitivities for SEA should not be overemphasized since the annual cycles in τ_a are out of phase (Figure 5).

We note that the mostly negative sensitivities computed for ModelE2 are in contrast to positive values of $\Delta\ln N/\Delta\ln\tau_a$ presented in *Quaas et al.* [2009] for ModelE. There are many differences between ModelE2 and ModelE. Thus, pinpointing which model change caused the shift in $\Delta\ln N/\Delta\ln\tau_a$ is impossible without performing an additional suite of many sensitivity simulations, which is beyond the scope of this study. In any

©2014 American Geophysical Union. All rights reserved.

Accepted Article

case, we summarize here the differences in ModelE and ModelE2 that likely contributed to differences in sensitivities presented here versus *Quaas et al*. The aerosol scheme in this study uses MATRIX (see Table 1), whereas that in Quaas et al. uses an aerosol scheme that tracks only mass concentrations [see *Menon et al.*, 2008]. Also, the first aerosol indirect effect was parameterized as an empirical relationship between *N* and aerosol number concentrations (obtained from aerosol mass for an assumed log-normal distribution [Menon and *Rotstayn* [2006]), whereas the parameterization used in our study is physically based (Table 1). As previously noted, ModelE2 does not include the second aerosol indirect effect whereas simulations for *Quaas et al.* included both the first and second indirect effects [see *Menon et al.*, 2008]. Overall changes to the model include an increase in spatial resolution from 4° x 5° to 2° x 2.5°, and changes to model physics described in *Schmidt et al.* [2006] for ModelE and *Schmidt et al.* [2014] for ModelE2. Additional reasons for differences between sensitivities presented in our paper versus *Quaas et al.* are in the Discussion, Section 4.4.

Carrying out sensitivity simulations to improve process-level understanding of the key drivers that determine aerosol-cloud interaction sensitivities is an important topic for future research.

Accepted Article

©2014 American Geophysical Union. All rights reserved.

3.4 Controlling for meteorology when assessing sensitivity of N to τ_a

In the previous section we used $\Delta\ln N/\Delta\ln\tau_a$ as a metric for assessing the first aerosol indirect effect. While this metric has been widely used by past studies, there is reason to believe that it may in some cases incorrectly diagnose aerosol indirect effects using large-scale observations and models. This is in part because both τ_a and N are sensitive to certain meteorological variables (see the Introduction). For example, continental air masses often have both higher anthropogenic aerosol loading and lower relative humidity than maritime air masses. Covariation between meteorological, cloud, and aerosol variables could lead to somewhat inaccurately attributing changes in N to τ_a.

In order to decouple aerosol and meteorological effects on N, we can use a statistical approach to assess the system as

$$\Delta\ln(N) = \Delta\ln(\tau_a)\left.\frac{\partial\ln(N)}{\partial\ln(\tau_a)}\right|_{\text{met}} + (\Delta met)\left.\frac{\partial\ln(N)}{\partial(met)}\right|_{\tau_a} \tag{6}$$

Where $\left.\frac{\partial\ln(N)}{\partial\ln(\tau_a)}\right|_{\text{met}}$ is the partial sensitivity of $\ln(N)$ to $\ln(\tau_a)$ at constant meteorology and $\left.\frac{\partial\ln(N)}{\partial\ln(\text{met})}\right|_{\tau_a}$ is the partial sensitivity of $\ln(N)$ to meteorology at constant τ_a. At this point, the term meteorology is used loosely and could represent any number of confounding meteorological variables at a variety of spatial scales. Dividing both sides by $\Delta\ln(\tau_a)$ results in

$$\frac{\Delta\ln(N)}{\Delta\ln(\tau_a)} = \left.\frac{\partial\ln(N)}{\partial\ln(\tau_a)}\right|_{\text{met}} + \frac{d(met)}{d\ln(\tau_a)}\left.\frac{\partial\ln(N)}{\partial(met)}\right|_{\tau_a} \tag{7}$$

©2014 American Geophysical Union. All rights reserved.

Accepted Article

The left hand side (LHS) represents the total sensitivity of ln(N) to ln(τ_a) (i.e. discussed in Section 3.3) and the first term on the right hand side (RHS) represents the partial sensitivity of ln(N) to ln(τ_a) at constant meteorology. We refer to these herein as "total" and "partial" sensitivities, respectively. The latter is a more direct indicator of how cloud microphysics responds to τ_a excluding any number of confounding metrological factors. The second term on the RHS of Eq. 7 represents the meteorological variables that cause differences between partial and total sensitivities. It is important to note that this term is nonzero only for meteorological variables that affect both N and τ_a; thus differences in partial versus total sensitivities are caused only by meteorological variables that affect both N and τ_a.

The partial sensitivities can be estimated using a multiple linear regression approach as

$$\ln(N_i) = u + \alpha \ln(\tau_{a,i}) + \sum_{j=1}^{p} \beta_j (met_{j,i}) + \varepsilon_i \tag{8}$$

where i is the sample index, j=1,2,…,p is the meteorological variable index, α is the partial sensitivity of ln(N) to ln(τ_a) that is of interest, *met* represents p different meteorological covariates, β is a vector representing the partial sensitivity of ln(N) to p different *met* variables, u is the intercept, and ε is the error vector (ε_i are uncorrelated and have equal variance). This statistical model follows the integral form of Eq. 6 (see the Auxiliary Material for more details). Similar approaches have been used in previous studies [e.g. *Kaufman et al.* 2005] for attempting to separate the impacts of aerosols and meteorology on cloud macrophysical properties.

©2014 American Geophysical Union. All rights reserved.

Accepted Article

Eq. (8) can be used to explore the impact of covariation between N , τ_a, and any number of meteorological variables or metrics. Here, we explore potential differences between total and partial sensitivity caused by changes in relative humidity at both the surface and 700 hPa. As discussed in the introduction, RH can directly alter τ_a via condensation of water onto aerosols, causing them to "swell". This effect is included in all three GCMs. RH of environmental air can also affect N. For example, the RH of free tropospheric air entrained into a cloud can affect its influence on N (see Introduction). While parameterizations have been proposed to account for this effect [e.g. *Barahona and Nenes*, 2007; *Barahona et al.*, 2011; *Ghan et al.*, 2011], they are not explicitly included in the three GCMs used in our study. (We note that in CAM5, entrainment is parameterized in the UW turbulence scheme, so may indirectly affect both the droplet activation process through the subgrid updraft velocity that is approximated using TKE (Table 1), and turbulent transport of hydrometeors.) In this analysis RH is determined directly using model values for simulated sensitivities, and from the ERA-Interim reanalysis for observed sensitivities (see Methods). As in *Barahona et al.*, grid cell average RH is assumed representative of the cloud-free air that would be entrained into the cloud. The changes in RH explored here for this near-coast marine region could be due to multiple pathways including large-scale shifts in prevailing winds.

Total and partial sensitivities for SAF during JJA are shown in Figure 7 (see the Auxiliary Material for numerical values). Including RH leads to a reduction in the MODIS observed sensitivity. This partial sensitivity is statistically indistinguishable from zero. For AM3 and CAM5, partial sensitivities are slightly lower than total

©2014 American Geophysical Union. All rights reserved.

Accepted Article

sensitivities but still statistically significant and larger than the observed sensitivity. The larger fractional difference between total and partial sensitivity for observations versus models may be in part due to the fact that RH alters microphysical properties of clouds via entrainment in reality (thus affecting the observations) while this process is not directly parameterized in the models used here. The ModelE2-simulated sensitivity remains indistinguishable from zero. We do not show results here for SEA because we are interested in sensitivities based on intraseasonal variation. See Section 4.2 for more discussion.

In general, Eq. (7) suggests that if the sensitivity of meteorology to τ_a and N to meteorology are the *same* sign (i.e. both positive or both negative), the partial sensitivity of N to τ_a will be lower than the total sensitivity. Alternatively, if the sensitivity of meteorology to τ_a and N to meteorology are of *opposite* sign (i.e. one positive and the other negative), the partial sensitivity of N to τ_a will be *higher* than the total sensitivity.

4.0 Discussion

4.1 Comparing parameterizations among the three GCMs

As shown in Figures 1, 4, and 5, spatial and temporal patterns of N and τ_a markedly differ among the three climate models used in this study. Horizontal winds are nudged in each model simulation. As such, differences among models and observations in aerosol and cloud fields are assumed to be dominated by differences in (1) aerosol schemes, (2) parameterizations of aerosol activation, and (3) cloud microphysics parameterizations.

©2014 American Geophysical Union. All rights reserved.

Accepted Article

It is interesting that while there are some differences in these parameterizations among the three models, they are overall quite similar (Table 1). The aerosol schemes represent the component that differs most among the models. Besides inherent differences in the parameterizations themselves (see Section 2.2), differences in assumptions regarding particle size distributions, hygroscopicity, and optical properties likely contribute to the discrepancies in aerosols and clouds presented here. The aerosol activation parameterizations are similar among the models though there are important differences in the subgrid treatments of vertical velocity, and assumptions on whether condensation occurs onto already existing cloud drops versus nucleating new ones (Table 1), both of which are likely key contributors to variations among the models. The cloud microphysics schemes are also similar among the models but differ in the number of sink pathways included for N (see Table 1).

Determining the relative importance of the aforementioned parameterizations for causing simulated differences in N and τ_a would require many sensitivity simulations, which is beyond the scope of the current study, but is an important topic for future research for bettering process-level understanding. For example, sensitivity simulations could be performed changing assumptions in each model on whether condensation grows already existing droplets versus nucleating new ones (see Table 1). We speculate that differences in this assumption could be an important contributor to N being generally higher in CAM5 than AM3.

We note that including the effects of entrainment on cloud microphysics in one model (not used in our study, NASA Global Modeling Initiative, GMI) has been shown to improve model versus satellite comparisons, especially in marine environments where

©2014 American Geophysical Union. All rights reserved.

Accepted Article

reductions in *N* from entrainment were shown to be large [*Barahona et al.*, 2011]. (See the Introduction and Section 3.4 for more details.)

It is also worth nothing that while there may exist differences between the observational datasets used for nudging (i.e. NCEP versus ERA-Interim reanalysis), we assume these differences are much smaller than those caused by the aforementioned parameterizations.

It is interesting to point out that global climate models appear to be moving away from empirically derived parameterizations for aerosol-cloud interactions (i.e. direct relationships for *N* as a function of only aerosol number concentrations) in favor of physically based ones that simulate activation of aerosols to cloud droplets based on the Köhler theory. While physically based parameterizations are more robust, they also introduce new complexity and dependence on accurately predicting (1) temporal and spatial patterns of size- and composition-resolved aerosol number concentrations, both of which alter hygroscopicity, and (2) local (cloud-scale) supersaturation, which is dependent on subgrid representations of vertical motions.

4.2 Comparing signatures of aerosol-cloud interactions in models versus observations

In the Introduction, Section 3.4, and Figure 7 we discuss how meteorology can confound apparent interactions for *N* and τ_a. We present one illustrative pathway for this confounding effect using variations in ambient RH, which can impact both *N* and τ_a . The effects of RH on τ_a are observed by MODIS and are parameterized in the models. However, while the effects on *N* occur in reality (thus affecting the

©2014 American Geophysical Union. All rights reserved.

Accepted Article

observations), they are not modeled in the GCMs used in this study (see Section 3.4). This points to additional difficulties in comparing observed versus modeled aerosol-cloud sensitivities using statistical relationships. The confounding influence of meteorology is only partially represented in the currently used physical parameterizations, while is of course fully represented in reality and thus the observations. (As an aside, the confounding effects of meteorology on *N* are not represented at all in older empirical parameterizations since they directly relate *N* to aerosol.) The extent to which confounding meteorological factors are represented in models can influence their "total" sensitivities. This can lead to differences in total sensitivities for models and observations that are not caused directly by differences in aerosol-cloud interactions, and could explain why the fractional difference in total versus partial sensitivity is much larger for observations than models (Figure 7). We also suggest that as models evolve and include more physically realistic process-based parameterizations, total aerosol-cloud sensitivities could change from inclusion of additional confounding meteorological factors even for constant aerosol indirect effect.

Evaluating new aerosol and cloud parameterizations in global climate models is important for narrowing the uncertainty in aerosol indirect effects. Satellite observations are well suited for such evaluations given their spatial and temporal coverage and resolution. However, as with most model versus observation comparisons, there are many inherent differences that make evaluation challenging. In an attempt to improve the comparison, we have used COSP to compute MODIS-simulated cloud properties for climate models and derived *N* identically to MODIS satellite observations. However, the fact that using large-scale observations to

©2014 American Geophysical Union. All rights reserved.

Accepted Article

attribute changes in cloud properties to aerosol-cloud interactions against meteorological variability is extremely difficult means that evaluation of new physically based aerosol-cloud parameterizations in GCMs challenging.

There are additional challenges involved in assessing aerosol-cloud interactions using large-scale observations that were not accounted for in this study. One example involves the use of vertically integrated observations, which requires the assumption that all detected aerosols and clouds are vertically collocated. Limited past observational studies suggest that the sensitivity of cloud microphysics to aerosol loading is higher when excluding aerosols that are vertically well separated from clouds [*Costantino and Breon*, 2010; *Costantino and Breon*, 2013]. It is of interest to pursue similar studies on the importance of vertical separation of clouds and aerosols using GCMs. Another challenge involves the use of τ_a as a proxy for CCN. This and past studies [e.g. *Quaas et al*., 2009] use τ_a since 1) it has been shown to be a reasonable proxy [*Andreae*, 2009], and 2) it is a relatively routine and certain satellite product. However, some studies have suggested that τ_a is a less than optimal aerosol proxy for investigating aerosol-cloud interactions [e.g. *Penner et al.*, 2011]. Aerosol Index (AI), which is the product of τ_a and Angstrom coefficient, has been suggested as a better proxy for CCN [e.g. see *Quaas and Boucher*, 2005 and references therein; *Penner et al.*, 2011]. We use τ_a since it has been more widely used in past studies including the most comprehensive model-satellite intercomparison of aerosol indirect effects to date [*Quaas et al*., 2009]. However, more detailed investigations on the suitability of τ_a, AI, or other new metrics as a proxy of CCN are of interest.

©2014 American Geophysical Union. All rights reserved.

4.3 Comparing satellite-simulated versus standard modeled values of *N*

In this investigation we have computed satellite-simulated values of *N* for GCMs. This provides an opportunity to compare satellite-simulated values of *N* to those from standard GCM output. Figure 8a shows the time series of vertical profiles for (in-cloud) *N* in SAF for CAM5. To maintain consistency with satellite-simulated *N*, values are from model time steps near Aqua overpass times (see Section 2.2). Also, when liquid cloud fraction is < 30% the entire column is screened and thus not included in the spatial mean for that time step. Individual grid cells with cloud fraction < 3% are screened to reduce noise. The color bar below the curtain plot shows satellite-simulated *N* for CAM5 using the same color scale as the vertical profiles; values are equivalent to those presented in Figure 5.

Figure 8a suggests that standard model values of *N* near cloud top in most cases appear to be lower than satellite-simulated *N*. To further quantify this difference, Figure 8b shows column maximum modeled *N* for each vertical profile versus satellite-simulated *N*. Satellite-simulated values of *N* are higher than standard model output with bias = 83 cm^{-3} and root mean square difference of 98 cm^{-3}. It is unclear whether this discrepancy stems from the COSP method for deriving liquid τ_c and r_e values, or from the algorithm for determining *N* from satellite-simulated values of liquid τ_c and r_e. This is an important topic for future research but is beyond the scope of this paper. However, the result has potentially important implications for using satellite observations to evaluate standard (not satellite-simulated) model output. It has been understood that assessing standard climate model output using satellite observations could be an inherently biased comparison due to differences in models

©2014 American Geophysical Union. All rights reserved.

Accepted Article

versus satellites [e.g. *Bodas-Salcedo et al*., 2011]. One might argue that these biases apply only to individual properties but that comparing sensitivities such as $\Delta \ln N / \Delta \ln \tau_a$ removes the bias since they depend only on *changes* in properties rather than their absolute values. However, the non-unity slope for the best fit presented in Figure 8b implies that even comparing sensitivities of standard model output versus observations may in some situations introduce bias. Versions of Figure 8b for SAF and SEA for both CAM5 and AM3 are in the Auxiliary Material; bias ranges from 55 to 115 cm^{-3}.

The aforementioned bias of 83 cm^{-3} is about half the difference in two-year mean MODIS observed versus MODIS-simulated *N* for CAM5 (i.e. 174 cm^{-3}, Table 2). Thus, a large fraction of the difference between observations and models reported here is from the technique for calculating *N* from satellite-simulated values. This raises interesting questions about the most suitable methods for evaluating cloud microphysics in climate models using standard climate model output versus satellite simulators. While the satellite-simulated technique employed in this study should minimize inherent model versus satellite biases, *N* from standard model output are nearer to expected values and include less computations with potential uncertainty.

4.4 Comparison to other studies

GCM-simulated aerosol indirect effects were evaluated against satellite observations in a previous model intercomparison by *Quaas et al*. [2009]. We build on this previous study and note that the GCMs evaluated here represent updated versions relative to those in *Quaas et al*. (See e.g. Section 3.3. for a description of model updates in ModelE2 relative to ModelE.) Consistent with results presented here for

©2014 American Geophysical Union. All rights reserved.

Accepted Article

CAM5, *Quaas et al.* showed that the modeled $\Delta\ln N/\Delta\ln\tau_a$ sensitivity over ocean regions was higher than MODIS-Aqua observations for various older configurations of CAM. Also, the sensitivity of AM3 used in our study was larger than observations, in contrast to the prototype version of AM3 used in *Quaas et al*. in which the sensitivity was lower than observations. As discussed in Section 3.3, sensitivities for ModelE2 were mostly negative in our study, whereas sensitivities for ModelE used in *Quaas et al.* were mostly positive. It is important to note that despite the similar range in the computed $\Delta\ln N/\Delta\ln\tau_a$ in our study versus *Quaas et al.*, results are not directly comparable due to the following differences in study design. First, we used different region definitions for calculating spatial means of aerosol and cloud quantities. $\Delta\ln N/\Delta\ln\tau_a$ depends on the spatial scale of data aggregation: all else being equal, the sensitivity is smaller when data are averaged over larger domains [*Sekiguchi et al*., 2003; *McComiskey et al*., 2009; *Quaas et al*., 2009]. Our study focuses on one particular type of cloud regime (i.e. maritime stratocumulus) and defines analysis regions to be small enough to ensure aerosol and cloud properties were mostly homogeneous within the regions, which has been shown to be important [*Grandey and Stier*, 2010; *Gryspeerdt and Stier*, 2012]. Second, due to a reduced number of analysis regions and models, we present regional and seasonal variations in $\Delta\ln N/\Delta\ln\tau_a$ for both models and observations. (*Quaas et al*. also present regional results in their supplemental material but is not the main focus of their analysis.) Third, computed uncertainty estimates for $\Delta\ln N/\Delta\ln\tau_a$ presented in our paper represent 95% confidence intervals for the specific time period and region, whereas the analysis in *Quaas et al*. represents the spread in seasonal and regional estimates. Confidence bounds presented in our investigation can be used to make statistical inferences on whether sensitivities derived using models versus observations are

©2014 American Geophysical Union. All rights reserved.

Accepted Article

significantly different from each other, and whether an individual sensitivity is distinguishable from zero. Fourth, we compute satellite-simulated model values of N whereas *Quaas et al*. use standard model output. We suggest that using modeled instead of satellite-simulated N may introduce biases in not only the evaluation of N but also $\Delta \ln N / \Delta \ln \tau_a$ (see Section 4.3), highlighting the need to minimize model-satellite discrepancies when evaluating aerosol indirect effects.

In general, the results presented here suggest that cloud microphysical properties appear more sensitive to aerosols in models than observations (noting the caveats discussed in previous sections), consistent with many previous studies as summarized by *McComiskey and Feingold* [2012].

5.0 Summary and conclusions

Accurately representing the interaction of atmospheric aerosols and clouds is a great challenge in global climate modeling. This is in part because many aerosol and cloud physical processes operate on spatial scales that are much smaller than climate model grid cells. Thus, these processes are represented in climate models using parameterizations, making estimates of aerosol indirect forcing uncertain. To reduce uncertainty and improve parameterizations, signatures of aerosol indirect effects from climate models can be compared to those measured by satellites. These comparisons require special attention since aerosol and cloud measurements from satellites are inherently different than standard climatological output from climate models.

In this study we compared aerosol and cloud properties in three global climate models (GFDL-AM3, NCAR-CAM5, and GISS-ModelE2) to MODIS Aqua satellite

©2014 American Geophysical Union. All rights reserved.

Accepted Article

observations. The period of focus was January 1, 2007 to January 1, 2009. In an attempt to elucidate differences in observations versus models caused by parameterizations directly related to aerosol and cloud processes, we (a) reduce inherent differences between satellite observations and climate models by computing MODIS-simulated cloud properties for the three GCMs using COSP, (b) extract model-simulated values for model time steps nearest MODIS overpass times using three hourly model output, and (c) reduce differences in observed versus modeled meteorology by nudging winds predicted by GCMs to observations. Coastal marine areas with persistent clouds off the west coast of South Africa (SAF) and east coast of Southeast Asia (SEA) were the focus of this study, though these regions were also presented in the context of global distributions.

We found that the three climate models captured quite well many spatial patterns of aerosol optical depths τ_a around the globe including local maxima in South America, central and northern Africa, Southeast Asia, and the eastern continental United States. Two-year mean values for all three models were lower than observations in SAF. Values in SEA were nearly the same, lower, and higher than observations for AM3, CAM5, and ModelE2, respectively. MODIS observations show a strong seasonal cycle in SAF for aerosol optical depth with maximum values up to around 1 in July, August, and September when biomass burning is prevalent. Modeled values of τ_a are near observations for most of the year though are underestimated during this burning season.

Cloud droplet number concentrations *N* were computed from observed liquid cloud optical depths and liquid droplet effective radii assuming clouds were adiabatically

©2014 American Geophysical Union. All rights reserved.

Accepted Article

stratified [*Bennartz*, 2007]. This algorithm was used consistently for both MODIS observations and satellite-simulated GCM results. All grid cells with liquid cloud fraction < 30% were screened to reduce noise in the algorithm and ensure the existence of large-scale liquid clouds. For all three models, simulated values of (in-cloud) *N* averaged over the entire period were higher in most ocean regions than observed values. In coastal marine environments such as SAF that experience high aerosol concentrations that act as CCN, values of observed *N* were higher than remote ocean regions, consistent with previously reported results [*Bennartz*, 2007, *Rausch et al*., 2010]. Both AM3 and CAM5 predicted this expected spatial pattern of higher *N* in near-coast regions versus remote ocean regions. Simulated values of *N* in SAF were somewhat higher, much higher, and somewhat lower than observations for AM3, CAM5, and ModelE2, respectively. In SEA, values simulated by AM3 and ModelE were somewhat higher than observations while values from CAM5 were much higher than observed. The time series of observed spatial means for SAF shows maximum *N* in JJA when biomass burning emissions are prevalent. CAM5 reproduces this seasonal cycle but with values for *N* higher than observed. Values simulated by AM3 are near observations while those from ModelE2 are near observed for the portions of the year that the model produces clouds in the region. (Values for ModelE2 are screened for most days in JJA due to liquid cloud fractions < 30% for all grid cells in SAF.) Differences between observed versus modeled *N* are caused by discrepancies in satellite observed versus simulated τ_c and r_e.

Signatures of microphysical aerosol-cloud interactions were assessed using $\Delta \ln N / \Delta \ln \tau_a$. This was computed using daily time series of satellite-observed and satellite-simulated regional mean results for SAF and SEA. For the entire two-year

©2014 American Geophysical Union. All rights reserved.

period in SAF, the sensitivity ($\Delta\ln N/\Delta\ln\tau_a$) computed for AM3 was statistically indistinguishable from observations. The sensitivity computed for CAM5 was higher than observations, while that for ModelE2 was statistically indistinguishable from zero. During JJA, the season with the most statistically robust results (see Section 3.3), $\Delta\ln N/\Delta\ln\tau_a$ for AM3 and CAM5 was higher than observed. The sensitivity for ModelE2 was indistinguishable from zero. In SEA, $\Delta\ln N/\Delta\ln\tau_a$ over the entire analysis period had similar observed versus modeled discrepancies as in SAF. Values for sensitivities in SEA were roughly two times larger than in SAF. $\Delta\ln N/\Delta\ln\tau_a$ during each season was statistically indistinguishable from zero.

Using the aforementioned "total" sensitivity, $\Delta\ln N/\Delta\ln\tau_a$, to assess the first indirect effect implicitly assumes that changes in τ_a and N are orthogonal to other factors such as meteorology. This may or may not be the case, however, since changes in N could be in fact caused by meteorological factors that also alter τ_a. A simple statistical framework for assessing the confounding effects of meteorological regime on the first aerosol indirect effect was presented. We provided an example pathway for how including the sensitivities of both N and τ_a to relative humidity can markedly change the computed sensitivity of N to τ_a, indicating that $\Delta\ln N/\Delta\ln\tau_a$ should be used with caution for assessing the first aerosol indirect effect using spatially coarse large-scale observations and models. Model parameterizations generally represent only a portion of the relevant influence of meteorology on clouds, which is an additional source of discrepancy for model versus observation comparisons. For example, entrainment of environmental air can alter N in reality and thus observations, but this process was not represented in the GCMs used here. This is further discussed in Section 4.3.

©2014 American Geophysical Union. All rights reserved.

Accepted Article

Satellite-simulated values of *N* were compared to standard model output in SAF for CAM5. (Additional comparisons are in the Auxiliary Material.) Standard model values were extracted from the same overpass time steps and subject to the same screening as satellite-simulated values. It was found that satellite-simulated *N* was higher than standard model output with a bias of 83 cm^{-3}. This indicates that satellite-simulated versus standard model values of *N* can be markedly different, with *N* derived from satellite-simulated model output more biased (compared to observations) than standard model output. A large fraction of the bias between satellite-observed versus simulated *N* reported here is from the technique for calculating *N* from satellite-simulated values, raising interesting questions about the most suitable methods for evaluating cloud microphysics from climate models (see Section 4.2), which is an important topic of future research.

Reducing the global scale uncertainty of climate forcing caused by interactions that occur at the microscale is inherently challenging. Global observations are needed for large-scale evaluation of models because conclusions can vary by the location (and size) of regions under investigation. However, satellite sensors view the atmosphere in inherently different ways than do climate models. In this paper we attempted to minimize some of these inherent differences to evaluate modeled aerosols, clouds, and their interactions, with a focus on cloud droplet number concentrations for marine clouds off the west and east coasts of South Africa and Southeast Asia, respectively. For future improvements in parameterizations of aerosol and cloud processes, it is important to evaluate and benchmark signatures of aerosol-cloud interactions in global climate models by comparing to observations using meaningful metrics. The

©2014 American Geophysical Union. All rights reserved.

Accepted Article

extreme difficulty in using large-scale observations to attribute changes in cloud properties to aerosol-cloud interactions against meteorological variability makes evaluation of new physically based aerosol-cloud parameterizations in GCMs challenging.

Acknowledgements

MODIS observations supporting Figures 1-5 and 8 are freely available from National Aeronautics and Space Administration. Global climate model data used for these figures may be made available upon request from the corresponding author. Data supporting Figures 6 and 7 can be found in the Auxiliary Material. The ERA-Interim reanalysis data are freely available from European Centre for Medium-Range Weather Forecasts.

GBW and SB were supported by the Department of Energy's (DOE) Earth System Modeling (ESM) Program via the FASTER project (FAst-physics System TEstbed and Research). LJ was supported by the NASA MAP program Modeling, Analysis and Prediction Climate Variability and Change (NNH08ZDA001N-MAP). XL and KZ were supported by the Office of Science of U.S. Department of Energy as part of the Earth System Modeling Program and the DOE SciDAC program on Applying Computationally Efficient Schemes for BioGeochemical Cycles (ACES4BGC). JHJ was supported by the Jet Propulsion Laboratory, California Institute of Technology, under contract by NASA. Work at Lawrence Berkeley National Laboratory was also supported by the U.S. Department of Energy's Earth System Modeling, an Office of Science, Office of Biological and Environmental Research program under Contract No. DE-AC02-05CH11231. The Pacific Northwest National Laboratory is operated

Accepted Article

©2014 American Geophysical Union. All rights reserved.

for DOE by Battelle Memorial Institute under contract DE-AC06-76RLO 1830. XL would like to acknowledge the use of computational resources (ark:/85065/d7wd3xhc) at the NCAR-Wyoming Supercomputing Center provided by the National Science Foundation and the State of Wyoming, and supported by NCAR's Computational and Information Systems Laboratory. SB acknowledges resources supporting this work by the NASA High-End Computing (HEC) Program through the NASA Center for Climate Simulation (NCCS) at Goddard Space Flight Center.

For helpful discussions and guidance we thank Surabi Menon (formerly of Lawrence Berkeley National Laboratory), David Romps and William Collins (Lawrence Berkeley National Laboratory and University of California, Berkeley), Gijs de Boer and Robert Pincus (NOAA Earth System Research Laboratory), Jennifer Kay (National Center for Atmospheric Research), and Yangang Liu (Brookhaven National Laboratory). We acknowledge the MODIS Science Team for processing and making publically available the satellite data used in this study. We also acknowledge ECMWF for the ERA-Interim reanalysis.

6.0 References

Abdul-Razzak, H. and S. J. Ghan (2000). "A parameterization of aerosol activation 2. Multiple aerosol types." Journal of Geophysical Research-Atmospheres **105**(D5): 6837-6844.

Andreae, M. O. (2009). "Correlation between cloud condensation nuclei concentration and aerosol optical thickness in remote and polluted regions." Atmospheric Chemistry and Physics **9**(2): 543-556.

©2014 American Geophysical Union. All rights reserved.

Accepted Article

Ban-Weiss, G. A., L. Cao, et al. (2012). "Dependence of climate forcing and response on the altitude of black carbon aerosols." Climate Dynamics **38**(5-6): 897-911.

Barahona, D., and A. Nenes (2007). "Parameterization of cloud droplet formation in large scale models: Including effects of entrainment." J. Geophys.Res., **112**, doi:10.1029/2007JD008473.

Barahona, D., R. Sotiropoulou, et al. (2011). "Global distribution of cloud droplet number concentration, autoconversion rate, and aerosol indirect effect under diabatic droplet activation." Journal of Geophysical Research-Atmospheres **116**.

Bauer, S. E., D. L. Wright, et al. (2008). "MATRIX (Multiconfiguration Aerosol TRacker of mIXing state): an aerosol microphysical module for global atmospheric models." Atmospheric Chemistry and Physics **8**(20): 6003-6035.

Bennartz, R. (2007). "Global assessment of marine boundary layer cloud droplet number concentration from satellite." Journal of Geophysical Research-Atmospheres **112**(D2).

Bennartz, R., J. W. Fan, et al. (2011). "Pollution from China increases cloud droplet number, suppresses rain over the East China Sea." Geophysical Research Letters **38**.

Bodas-Salcedo, A., M. J. Webb, et al. (2011). "COSP Satellite simulation software for model assessment." Bulletin of the American Meteorological Society **92**(8): 1023-1043.

Brenguier, J., H. Pawlowska, L. Schuller, R. Preusker, J. Fischer, and Y. Fouquart (2000) "Radiative properties of boundary layer clouds: Droplet effective

©2014 American Geophysical Union. All rights reserved.

Accepted Article

radius versus number concentration". J. Atmos. Sci., **57**, 803–821.

Costantino, L. and F.-M. Breon (2010). "Analysis of aerosol-cloud interaction from multi-sensor satellite observations." Geophysical Research Letters **37**.

Costantino, L. and F. M. Breon (2013). "Aerosol indirect effect on warm clouds over South-East Atlantic, from co-located MODIS and CALIPSO observations." Atmospheric Chemistry and Physics **13**(1): 69-88.

de Boer, G., S. E. Bauer, et al. (2013). "Evaluation of aerosol-cloud interaction in the GISS ModelE using ARM observations." Journal of Geophysical Research-Atmospheres **118**(12): 6383-6395.

Del Genio, A. D., M.-S. Yao, W. Kovari, and K.-W. Lo (1996). "A prognostic cloud water parameterization for global climate models." Journal of Climate, **9**, 270–304.

Del Genio, A.D., Y. Chen, D. Kim, and M.S. Yao (2012). "The MJO Transition from Shallow to Deep Convection in CloudSat/CALIPSO Data and GISS GCM Simulations." *J Climate*, *25*(11), 3755–3770, doi:10.1175/JCLI-D-11-00384.1.

Donner, L. J., B. L. Wyman, et al. (2011). "The Dynamical Core, Physical Parameterizations, and Basic Simulation Characteristics of the Atmospheric Component AM3 of the GFDL Global Coupled Model CM3." Journal of Climate **24**(13): 3484-3519.

Duynkerke, P., H. Zhang, and P. Jonker (1995). "Microphysical and turbulent structure of nocturnal stratocumulus as observed during ASTEX." J. Atmos. Sci., **52**, 2763–2777.

Accepted Article

©2014 American Geophysical Union. All rights reserved.

Engström, A. and A. M. L. Ekman (2010). “Impact of meteorological factors on the correlation between aerosol optical depth and cloud fraction.” Geophysical Research Letters 37.

Feingold, G., W. L. Eberhard, et al. (2003). "First measurements of the Twomey indirect effect using ground-based remote sensors." Geophysical Research Letters **30**(6).

Feingold, G., L. A. Remer, et al. (2001). "Analysis of smoke impact on clouds in Brazilian biomass burning regions: An extension of Twomey's approach." Journal of Geophysical Research-Atmospheres **106**(D19): 22907-22922.

Fountoukis, C. and A. Nenes, A. (2005). “Continued Development of a Cloud Droplet Formation Parameterization for Global Climate Models.” Journal of Geophysical Research-Atmospheres, **110**, doi:10.1029/2004JD005591.

Fu, W., J. Guo, Y. Wu et al., (2014). “Satellite Observed Aerosol-Induced Variability in Warm Cloud Properties under Different Meteorological Conditions over Eastern China.” Atmosphere Environment. **84**, 122-132.

Gates, W. L. (1992). AMIP: The Atmospheric Model Intercomparison Project. Bull. Amer. Meteor. Soc. **73:** 1962-1970.

Gates, W. L., et al. (1999) “An overview of the results of the Atmospheric Model Intercomparison Project (AMIP I).” Bull. Amer. Meteor. Soc. **80**, 29-55.

George, R. C. and R. Wood (2010). "Subseasonal variability of low cloud radiative properties over the southeast Pacific Ocean." Atmospheric Chemistry and Physics **10**(8): 4047-4063.

Accepted Article

©2014 American Geophysical Union. All rights reserved.

Gettelman, A., X. Liu, et al. (2010). "Global simulations of ice nucleation and ice supersaturation with an improved cloud scheme in the Community Atmosphere Model." Journal of Geophysical Research-Atmospheres **115**.

Gettelman, A., H. Morrison, et al. (2008). "A new two-moment bulk stratiform cloud microphysics scheme in the community atmosphere model, version 3 (CAM3). Part II: Single-column and global results." Journal of Climate **21**(15): 3660-3679.

GFDL Global Atmosphere Model Development Team. (2004): "The new GFDL global atmosphere and land model AM2-LM2: Evaluation with prescribed SST simulations." J. Climate, **17**, 4641-4673, doi:10.1175/JCLI-3223.1.

Ghan, S.J., L. R. Leung, and R. C. Easter. (1997). "Prediction of cloud droplet number in a general circulation model." J. Geophys. Res., **102**, doi:10.1029/97JD01810.

Ghan SJ, H Abdul-Razzak, A Nenes, Y Ming, X Liu, M Ovchinnikov, B Shipway, N Meskhidze, J Xu, and X Shi. (2011). "Droplet Nucleation: Physically-Based Parameterization and Comparative Evaluation." Journal of Advances in Modeling Earth Systems **3**. doi:10.1029/2011MS000074

Giorgi, F., and W. L. Chameides (1985) "The rainout parameterization in a photochemical model." J. Geophys. Res., **90**, 7872–7880.

Ginoux, P., M. Chin, I. Tegen, J. M. Prospero, B. Holben, O. Dubovik, and S.-J. Lin (2001), "Sources and distributions of dust aerosols simulated with the GOCART model." J. Geophys. Res., **106**, 20,255–20,273.

Ginoux, P., L. W. Horowitz, V. Ramaswamy, I. V. Geogdzhayev, B. N. Holben, G. Stenchikov, and X. Tie (2006), "Evaluation of aerosol distribution and

Accepted Article

©2014 American Geophysical Union. All rights reserved.

optical depth in the Geophysical Fluid Dynamics Laboratory coupled model CM2.1 for present climate." J. Geophys. Res., **111**, D22210, doi:10.1029/2005JD006707.

Golaz, J.-C., M. Salzmann, L. J. Donner, L. W. Horowitz, Y. Ming, and M. Zhao (2011) "Sensitivity of the aerosol indirect effect to subgrid variability in the cloud parameterization of the GFDL Atmosphere General Circulation Model AM3." J. Climate, **24**, 1-6. doi: 10.1175/2010JCLI3945.1.

Grandey, B. S. and P. Stier (2010). "A critical look at spatial scale choices in satellite-based aerosol indirect effect studies." Atmos. Chem. Phys., **10**, 11459-11470.

Gryspeerdt**,** E**.** and P. Stier (2012). "Regime-based analysis of aerosol-cloud interactions." Geophysical Research Letters, **39**, doi: 10.1029/2012GL053221**.**

Guo, H., J.-C. Golaz, L. J. Donner, P. Ginoux, and R. S. Hemler (2014). "Multi-variate probability density functions with dynamics in the GFDL atmospheric general circulation model: Global Tests." *J. Climate*, **27**, 2087-2108, doi: 10.1175/JCLI-D-13-00347.1

Hansen, J., M. Sato, et al. (2005). "Efficacy of climate forcings." Journal of Geophysical Research-Atmospheres **110**(D18).

IPCC (2007), Climate Change 2007: The Physical Science Basis. Contribution of Working Group I to the Fourth Assessment Report of the Intergovernmental Panel on Climate Change, edited by S. Solomon et al., Cambridge Univ. Press, Cambridge, U. K.

IPCC (2013) Climate Change 2013: The Physical Science Basis. Contribution of Working Group I to the Fifth Assessment Report of the Intergovernmental

Accepted Article

©2014 American Geophysical Union. All rights reserved.

Panel on Climate Change [Stocker, T.F., D. Qin, G.-K. Plattner, M. Tignor, S.K. Allen, J. Boschung, A. Nauels, Y. Xia, V. Bex and P.M. Midgley (eds.)]. Cambridge University Press, Cambridge, United Kingdom and New York, NY, USA, 1535 pp.

Jiang, J.H., H. Su, M. Schoeberl, S.T. Massie, P. Colarco, S. Platnick, and N. Livesey, (2008). "Clean and polluted clouds: relationships among pollution, ice cloud and precipitation in South America," Geophys. Res. Lett. 35, L14804, doi:10.1029/2008GL034631, 2008.

Jiang, J.H., H. Su, C. Zhai, S.T. Massie, M.R. Schoeberl, P.R. Colarco, S. Platnick, Y. Gu, and K.N. Liou (2011) "Influence of convection and aerosol pollution on ice cloud particle effective radius," Atmos. Chem. Phys. **11**, 457-463. doi:10.5194/acp-11-457-2011

Kalnay, E., M. Kanamitsu, R. Kistler, W. Collins, D. Deaven, L. Gandin, M. Iredell, S. Saha, J. Woollen, Y. Zhu, M. Chelliah, W. Ebisuzaki, W. Higgins, J. Janowiak, K. C. Mo, C. Ropelewski, J. Wang, A. Leetmaa, R. Reynolds, Roy Jenne, and Dennis Joseph (1996) "The NCEP/NCAR 40-year reanalysis project" Bull. Amer. Meteor. Soc., **77**, 437-470.

Kaufman, Y. J., I. Koren, et al. (2005). "The effect of smoke, dust, and pollution aerosol on shallow cloud development over the Atlantic Ocean." Proceedings of the National Academy of Sciences of the United States of America **102,** 11207-11212.

Kay, J. E., B. R. Hillman, et al. (2012). "Exposing Global Cloud Biases in the Community Atmosphere Model (CAM) Using Satellite Observations and

Accepted Article

©2014 American Geophysical Union. All rights reserved.

Their Corresponding Instrument Simulators." Journal of Climate **25**(15): 5190-5207.

Khairoutdinov, M. F., and Y. L. Kogan. (2000). “A new cloud physics parameterization in a large-eddy simulation model of marine stratocumulus.” Mon. Wea. Rev., **128**, 229-243.

Kim, B.-G., S. Klein, and J. Norris (2005). “Continental liquid water cloud variability and its parameterization using Atmospheric Radiation Measurement data.” J. Geophys. Res., 110, D15S08, doi:10.1029/2004JD005122.

Kim, B., M. Miller, S. Schwartz, Y. Liu, and Q. Min (2008), “The role of adiabaticity in the aerosol first indirect effect” J. Geophys. Res., **113**, doi:10.1029/2007JD008961.

Kim, D., A.H. Sobel, A. Del Genio, Y.-H. Chen, S.J. Camargo, M.-S. Yao, M. Kelley, and L. Nazarenko (2012) “The tropical subseasonal variability simulated in the NASA GISS general circulation model”. J. Climate, **25**, 4641-4659. doi:10.1175/JCLI-D-11-00447.1.

Koch, D., G. A. Schmidt, et al. (2006). "Sulfur, sea salt, and radionuclide aerosols in GISS ModelE." Journal of Geophysical Research-Atmospheres **111**(D6).

Koren, I., G. Feingold, et al. (2010). "The invigoration of deep convective clouds over the Atlantic: aerosol effect, meteorology or retrieval artifact?" Atmospheric Chemistry and Physics **10**(18): 8855-8872.

Kumar, P., I. N. Sokolik, et al. (2009). "Parameterization of cloud droplet formation for global and regional models: including adsorption activation

Accepted Article

©2014 American Geophysical Union. All rights reserved.

from insoluble CCN." Atmospheric Chemistry and Physics **9**(7): 2517-2532.

Lamarque, J. F., T. C. Bond, et al. (2010). "Historical (1850-2000) gridded anthropogenic and biomass burning emissions of reactive gases and aerosols: methodology and application." Atmospheric Chemistry and Physics **10**(15): 7017-7039.

Li, F., P. Ginoux, and V. Ramaswamy (2008) "Distribution, transport, and deposition of mineral dust in the Southern Oceanand Antarctica: Contribution of major sources." J. Geophys. Res., **113**, D10207, doi:10.1029/2007JD009190.

Liu, X., J. E. Penner, S. J. Ghan, and M. Wang (2007). "Inclusion of Ice Microphysics in the NCAR Community Atmospheric Model Version 3 (CAM3)". Journal of Climate. ***20***, 4526-4547.

Liu, X., R. C. Easter, et al. (2012). "Toward a minimal representation of aerosols in climate models: description and evaluation in the Community Atmosphere Model CAM5." Geoscientific Model Development **5**(3): 709-739.

Lohmann, U. and J. Feichter (2005). "Global indirect aerosol effects: a review." Atmospheric Chemistry and Physics **5**: 715-737.

Manton, M. J., and W. R. Cotton (1977). "Formulation of approximate equations for modeling moist deep convection on the mesoscale." Department of Atmospheric Science Paper 266, Colorado State University, 62 pp.

Accepted Article

©2014 American Geophysical Union. All rights reserved.

Marshak, A., S. Platnick, et al. (2006). "Impact of three-dimensional radiative effects on satellite retrievals of cloud droplet sizes." Journal of Geophysical Research-Atmospheres **111**(D9).

Marshak, A., G. Wen, et al. (2008). "A simple model for the cloud adjacency effect and the apparent bluing of aerosols near clouds." Journal of Geophysical Research-Atmospheres **113**(D14).

McComiskey, A. and G. Feingold (2012). "The scale problem in quantifying aerosol indirect effects." Atmospheric Chemistry and Physics **12**(2): 1031-1049.

McComiskey, A., G. Feingold, et al. (2009). "An assessment of aerosol-cloud interactions in marine stratus clouds based on surface remote sensing." Journal of Geophysical Research-Atmospheres **114**.

Menon, S. (2004). "Current uncertainties inassessing aerosol effects on climate." Annual Review of Environment and Resources **29**: 1-30.

Menon, S., and L. Rotstayn (2006). “The radiative influence of aerosol effects on liquid-phase cumulus and stratus clouds based on sensitivity studies with two climate models.” Clim. Dyn., **27**, 345–356.

Menon, S., A. D. Del Genio, et al. (2008). "Analyzing signatures of aerosol-cloud interactions from satellite retrievals and the GISS GCM to constrain the aerosol indirect effect." Journal of Geophysical Research-Atmospheres **113**(D14).

Menon, S., D. Koch, et al. (2010). "Black carbon aerosols and the third polar ice cap." Atmospheric Chemistry and Physics **10**(10): 4559-4571.

Accepted Article

©2014 American Geophysical Union. All rights reserved.

Miller, R. L., R. V. Cakmur, et al. (2006). "Mineral dust aerosols in the NASA goddard institute for Space Sciences ModelE atmospheric general circulation model." Journal of Geophysical Research-Atmospheres **111**(D6).

Min, Q., E. Joseph, et al. (2012). "Comparison of MODIS cloud microphysical properties with in-situ measurements over the Southeast Pacific." Atmospheric Chemistry and Physics **12**(23): 11261-11273.

Ming, Y., V. Ramaswamy, et al. (2006). "A new parameterization of cloud droplet activation applicable to general circulation models." Journal of the Atmospheric Sciences **63**(4): 1348-1356.

Ming, Y., V. Ramaswamy, L. J. Donner, V. T. J. Phillips, S. A. Klein, P. A. Ginoux, and L. W. Horowitz (2007) "Modeling the interactions between aerosols and liquid water clouds with a self-consistent cloud scheme in a General Circulation Model". J. Atmos. Sci., **64**, 1189-1209. doi:10.1175/JAS3874.1.

Monahan, E. C., D. E. Spiel, and K. L. Davidsona (1986) "A model of marine aerosol generation via whitecaps and wave disruption." Oceanic Whitecaps, E. C. Monahan and G. Mac Niocaill, Eds., D. Reidel, 167–174.

Morrison, H. and A. Gettelman (2008). "A New Two-Moment Bulk Stratiform Cloud Microphysics Scheme in the Community Atmosphere Model, Version 3 (CAM3). Part I: Description and Numerical Tests." Journal of Climate **21**(15): 3642-3659.

Morrison, H. and W. W. Grabowski (2008). "Modeling supersaturation and subgrid-scale mixing with two-moment bulk warm microphysics." Journal of the Atmospheric Sciences **65**(3): 792-812.

Accepted Article

©2014 American Geophysical Union. All rights reserved.

Myhre, G., F. Stordal, et al. (2007). "Aerosol-cloud interaction inferred from MODIS satellite data and global aerosol models." Atmospheric Chemistry and Physics **7**(12): 3081-3101.

Nakajima T.Y., Suzuki K., Stephens G.L. (2010) "Droplet Growth in Warm Water Clouds Observed by the A-Train. Part I: Sensitivity Analysis of the MODIS-Derived Cloud Droplet Sizes" Journal of the Atmospheric Sciences, **67**, 1884-1896.

Neale, R. B., et al. (2010). Description of the NCAR Community Atmosphere Model (CAM 5.0), NCAR Tech. Note NCAR/TN-486+STR, 268 pp., Natl. Cent. for Atmos. Res., Boulder, Colo., available at http://www.cesm.ucar.edu/models/cesm1.0/cam/

Nenes, A. and J. H. Seinfeld (2003). "Parameterization of cloud droplet formation in global climate models." Journal of Geophysical Research-Atmospheres **108**(D14).

Ovtchinnikov, M., and S. J. Ghan (2005). "Parallel simulations of aerosol influence on clouds using cloud-resolving and single-column models." J. Geophys. Res., 110, D15S10, doi:10.1029/2004JD005088.

Park, S., C.S. Bretherton (2009). "The University of Washington Shallow Convection and Moist Turbulence Schemes and Their Impact on Climate Simulations with the Community Atmosphere Model." *J. Climate*, **22**, 3449–3469.
doi: 10.1175/2008JCLI2557.1

Park, S., C. S. Bretherton, P. Rasch (submitted). "Global Cloud Simulation in the Community Atmosphere Model, version 5. Journal of Climate.

Accepted Article

©2014 American Geophysical Union. All rights reserved.

Pawlowska, H., J. L. Brenguier, et al. (2000). "Microphysical properties of stratocumulus clouds." Atmospheric Research **55**(1): 15-33.

Penner, J.E., L. Xu, M. Wang. (2011). "Satellite methods underestimate indirect climate forcing by aerosols." Proceedings of the National Academy of Sciences of the United States of America, **108**, 13404-13408.

Petters, J. L., H. Jiang, et al. (2013). "A comparative study of the response of modeled non-drizzling stratocumulus to meteorological and aerosol perturbations." Atmospheric Chemistry and Physics **13**(5): 2507-2529.

Pincus, R., S. Platnick, S. A. Ackerman, R. S. Hemler, and R. J. P. Hofmann (2012) "Reconciling simulated and observed views of clouds: MODIS, ISCCP, and the limits of instrument simulators." J. Climate, 25, 4699-4720. doi:10.1175/JCLI-D-11-00267.1

Platnick, S., et al. (2003). "The MODIS cloud products: Algorithms and examples from Terra" IEEE Trans. Geosci. Remote Sens., 41, 459–473.

Pruppacher, H. R., and J. D. Klett (1997). "Microphysics of Clouds and Precipitation." Kluwer Academic Publishers, Dordrecht. 954 pp.

Quaas, J. and O. Boucher (2005). "Constraining the first aerosol indirect radiative forcing in the LMDZ GCM using POLDER and MODIS satellite data." Geophysical Research Letters **32**(17).

Quaas, J., O. Boucher, et al. (2006). "Constraining the total aerosol indirect effect in the LMDZ and ECHAM4 GCMs using MODIS satellite data." Atmospheric Chemistry and Physics **6**: 947-955.

Accepted Article

©2014 American Geophysical Union. All rights reserved.

Quaas, J., Y. Ming, et al. (2009). "Aerosol indirect effects - general circulation model intercomparison and evaluation with satellite data." Atmospheric Chemistry and Physics **9**(22): 8697-8717.

Quaas, J., B. Stevens, et al. (2010). "Interpreting the cloud cover - aerosol optical depth relationship found in satellite data using a general circulation model." Atmospheric Chemistry and Physics **10**(13): 6129-6135.

Ramanathan, V., P. J. Crutzen, et al. (2001). "Atmosphere - Aerosols, climate, and the hydrological cycle." Science **294**(5549): 2119-2124.

Rausch, J., A. Heidinger, et al. (2010). "Regional assessment of microphysical properties of marine boundary layer cloud using the PATMOS-x dataset." Journal of Geophysical Research-Atmospheres **115**.

Rayner, N. A., Parker, D. E.; Horton, E. B.; Folland, C. K.; Alexander, L. V.; Rowell, D. P.; Kent, E. C.; Kaplan, A. (2003) “Global analyses of sea surface temperature, sea ice, and night marine air temperature since the late nineteenth century.” J. Geophys. Res. **108**, DOI: 10.1029/2002JD002670.

Remer, L. A., Y. J. Kaufman, et al. (2005). "The MODIS aerosol algorithm, products, and validation." Journal of the Atmospheric Sciences **62**(4): 947-973.

Rosenfeld, D. and G. Feingold (2003). "Explanation of discrepancies among satellite observations of the aerosol indirect effects." Geophysical Research Letters **30**(14).

Rotstayn, L. D., (1997). “A physically based scheme for the treatment of stratiform clouds and precipitation in large-scale models. I: Description and evaluation of the microphysical processes.” Q. J. R. Meteorol. Soc., **123**, 1227-1282.

Rotstayn, L., B. F. Ryan, and J. J. Katzfey (2000). “A scheme for calculation of the

©2014 American Geophysical Union. All rights reserved.

Accepted Article

liquid fraction in mixed-phase stratiform clouds in large-scale models." Mon. Wea. Rev., **128**, 1070-1088.

Schmidt, G. A., M. Kelley, et al. (2014). "Configuration and assessment of the GISS ModelE2 contributions to the CMIP5 archive." J. Adv. Model. Earth Syst., doi:10.1002/2013MS000265. *In press.*

Sekiguchi, M., T. Nakajima, et al. (2003). "A study of the direct and indirect effects of aerosols using global satellite data sets of aerosol and cloud parameters." Journal of Geophysical Research-Atmospheres **108**(D22).

Tiedtke, M. (1993). "Representation of clouds in large-scale models." *Mon. Wea. Rev.*, **121**, 3040–3061.

Twohy, C. H., J. A. Coakley, et al. (2009). "Effect of changes in relative humidity on aerosol scattering near clouds." Journal of Geophysical Research-Atmospheres **114**.

Twohy, C. H., M. D. Petters, et al. (2005). "Evaluation of the aerosol indirect effect in marine stratocumulus clouds: Droplet number, size, liquid water path, and radiative impact." Journal of Geophysical Research-Atmospheres **110**(D8).

Twomey, S. (1977). "Influence of Pollution on Shortwave Albedo of Clouds." Journal of the Atmospheric Sciences **34**(7): 1149-1152.

Voldoire, A. et al. (2012). "The CNRM-CM5.1 global cli- mate model: Description and basic evaluation." Climate Dyn., **40**, 2091–2121, doi:10.1007/s00382-011-1259-y.

Wood, R., Comstock, K. K., Bretherton, C. S., Cornish, C., Tomlinson, J., Collins, D.

Accepted Article

©2014 American Geophysical Union. All rights reserved.

R., and Fairall, C. (2008). "Open cellular structure in marine stratocumulus sheets," J. Geophys. Res.-Atmos., **113**, doi:10.1029/2007jd009371.

Yao, M.S., and Y. Cheng (2012). "Cloud Simulations in Response to Turbulence Parameterizations in the GISS Model E GCM." *J Climate*, *25*(14), 4963–4974, doi:10.1175/JCLI-D-11-00399.1.

Zhang, M. H., Lin, W. Y., Klein, S. A., Bacmeister, J. T., Bony, S., Cederwall, R. T., Del Genio, A. D., Hack, J. J., Loeb, N. G., Lohmann, U., Minnis, P., Musat, I., Pincus, R., Stier, P., Suarez, M. J., Webb, M. J., Wu, J. B., Xie, S. C., Yao, M. S., and Zhang, J. H. (2005) "Comparing clouds and their seasonal variations in 10 atmospheric general circulation models with satellite measurements," J. Geophys. Res. Atmos., **110**, doi:10.1029/2004jd005021, 2005.

Zhang, Z., and S. Platnick (2011) An assessment of differences between cloud effective particle radius retrievals for marine water clouds from three MODIS spectral bands, J. Geophys. Res., **116**. doi:10.1029/2011JD016216.

Zhao C., S. A. Klein, S. Xie, X. Liu, J. Boyle, and Y. Zhang (2012). "Aerosol first indirect effects on non-precipitating low-level liquid cloud properties as simulated by CAM5 at ARM sites." Geophysical Research Letters." **39**, doi:10.1029/2012GL051213.

Accepted Article

©2014 American Geophysical Union. All rights reserved.

Accepted Article

Table 1. Summary of aerosol and warm cloud parameterizations for the three global climate models used in this study.

	AM3	CAM5	ModelE2
Aerosol scheme	• Predicts mass distributions of major aerosol components. Number concentrations are computed from assumed size distributions. • Further described in Section 2.2 and *Donner et al.* [2011].	• Modal Aerosol Module (MAM3) represents three lognormal aerosol modes: Aitken, Accumulation, and Coarse. The three aerosol modes represent multiple species. See Section 2.2 and *Liu et al.* [2012].	• MATRIX [*Bauer et al.*, 2008] is an aerosol microphysical scheme based on the quadrature method of moments. The mixing state of 16 aerosol populations is tracked.
Aerosol activation in the GCM grid cell	• The number of activated cloud drops N^* is computed based on aerosol properties and supersaturation using Köhler theory [*Ming et al.* 2006; *Donner et al.* 2011]. • $N^*(a_1,\ldots,a_n,T,p,w)$ is the number of aerosols predicted to activate at the cloud scale, as a function of aerosol properties $a_1,\ldots,a_n$, temperature (T), pressure (p), and vertical velocity (w) • $\overline{N^*}$, the number of aerosols predicted to activate in a large-scale model grid box, is computed as $\overline{N^*} = \int N^*(a_1,\ldots,a_n,T,p,w)\,\mathrm{pdf}(w)\,dw$ where pdf(w), the subgrid distribution of w, is assumed to follow a normal distribution with mean corresponding to w that drives large-scale condensation (Tiedtke 1993). More details are in *Golaz et al.* [2011]. The integration is performed over the cloudy portion of the grid cell. • The standard deviation of pdf(w) is a function of eddy diffusivity (first suggested by *Ghan et al.* [1997]), with a lower bound of 0.7 m s^{-1}, which is higher than some past studies (see *Golaz et al.* [2011]). • The source term for grid-box mean cloud droplet number $\overline{N_d}$ from particle activation is computed as $\left.\frac{\partial \overline{N_d}}{\partial t}\right\|_{\text{activation}} = \overline{N^*}\frac{\partial C}{\partial t}$ when $\frac{\partial C}{\partial t} > 0$ where C is large scale cloud amount. Condensation into already existing clouds grows drops rather than nucleating new ones [*Ming et al., Golaz et al.*].	• Activation of (stratiform) cloud droplets from multimodal lognormal aerosol size distributions are based on Köhler theory [*Abdul Razzak and Ghan, 2000*]. • $\overline{N^*}$ is computed similarly to AM3 but using a subgrid characteristic vertical velocity rather than pdf (w), $\overline{N^*} = N^*(a_1,\ldots,a_2,T,p,\hat{w})$ • $\hat{w} = \max(\sqrt{0.667 * TKE}, 0.2)$ is the subgrid characteristic vertical velocity, where TKE is the turbulent kinetic energy diagnosed from the UW turbulence scheme [*Neale et al., 2010; Park and Bretherton, 2009*]. • The lower bound for $\hat{w}$ is 0.2 m s^{-1}. • $\left.\frac{\partial \overline{N_d}}{\partial t}\right\|_{\text{activation}}$ is calculated according to Appendix B in *Ovtchinnikov and Ghan*, (2005). Droplets can be activated in both newly-formed and preexisting stratiform clouds. For preexisting clouds, droplet activation is assumed to occur when and only at cloud base. For newly formed clouds, activation can occur at all levels wherever — . Vertical mixing of droplet number is coupled to the droplet activation source term. (CAM5 does not include prognostic droplet number in shallow or deep convective clouds.)	• As with CAM5, activation of cloud droplets is from *Abdul Razzak and Ghan* [2000]. • $\left.\frac{\partial \overline{N_d}}{\partial t}\right\|_{\text{activation}}$ is the same as for CAM5.

©2014 American Geophysical Union. All rights reserved.

Accepted Article

Cloud micro-physics	• All cloud microphysics (other than activation, described above) follow *Rotstayn* [1997] and *Rotstayn et al.* [2000], as described in Global Atmosphere Model Development Team [2004] for AM2. Prognostic $\overline{N_d}$ is determined from $\frac{\partial \overline{N_d}}{\partial t} = \left.\frac{\partial \overline{N_d}}{\partial t}\right\|_{\text{adv}} + \left.\frac{\partial \overline{N_d}}{\partial t}\right\|_{\text{mix}} + \left.\frac{\partial \overline{N_d}}{\partial t}\right\|_{\text{activation}} + \left.\frac{\partial \overline{N_d}}{\partial t}\right\|_{\text{sinks}}$ where the first two terms on RHS represent changes due to advection and turbulent mixing, third is activation (see cell above), and the last term is sinks. • Sinks included are evaporation, freezing, and autoconversion (see cell below). • Large-scale clouds can also acquire liquid water mass and number through detrainment from shallow convective clouds. • *N* is not predicted for deep convective clouds.	• Warm stratiform cloud microphysics (other than activation, described above) follow *Morrison and Gettelman* [2008]. • $\frac{\partial \overline{N_d}}{\partial t}$ is similar to AM3 but with more sink terms including e.g. accretion of cloud water, self collection of rain drops, and collection of rain by snow [*Morrison and Gettelman*, 2008]. • Vertical mixing moves water out of stratiform clouds where it evaporates. *N* is mixed out of the base and top of clouds, but is only fully depleted if there is no cloud water.	• $\frac{\partial \overline{N_d}}{\partial t}$ for warm stratiform clouds is similar to CAM5 but is a simplified version of *Morrison and Gettelman* [2008], including only the following sink terms: autoconversion, contact nucleation, and immersion freezing.
Auto-conversion	• A function of liquid water mixing ratio, *N*, and is only active above a critical liquid water amount with a corresponding threshold droplet radius of 8.2 μm, reduced from 10.6 μm used in AM2 [*Donner et al.*, 2011]. • Based on *Manton and Cotton* [1977], described in *Golaz et al.* [2011].	• A function of cloud water content and *N*, with no minimum threshold for initiation. • Based on *Khairoutdinov and Kogan* [2000]	• A function of condensate but not *N* or aerosol. As such, only the first aerosol indirect effect is included in the simulations. • Based on Del Genio et al. [1996], and described in 'Exp N' in *Menon et al.*, [2008].

©2014 American Geophysical Union. All rights reserved.

Accepted Article

Table 2. Two-year means ± standard deviation for the time series shown in Figure 5.

Region	Source	Liquid cloud fraction unscreened (%)	Liquid cloud fraction screened (%)	Liquid cloud optical depth τ_c (unitless)	Liquid cloud droplet effective radius r_e (μm)	Cloud thickness H (m)	Cloud droplet number concentration N (cm^{-3})	Aerosol optical depth τ_a (unitless)
SAF								
	MODIS observations	47 ± 18	73 ± 9	7 ± 1	13 ± 2	245 ± 30	69 ± 24	0.29 ± 0.26
	AM3	37 ± 13	70 ± 7	6 ± 2	10 ± 1	192 ± 32	136 ± 32	0.22 ± 0.08
	CAM5	44 ± 15	69 ± 9	8 ± 2	8 ± 1	214 ± 33	243 ± 84	0.19 ± 0.07
	ModelE2	17 ± 10	53 ± 10	12 ± 5	17 ± 3	361 ± 87	50 ± 27	0.16 ± 0.08
SEA								
	MODIS observations	26 ± 16	63 ± 10	15 ± 6	15 ± 2	366 ± 59	75 ± 32	0.25 ± 0.09
	AM3	26 ± 18	60 ± 12	14 ± 7	12 ± 3	321 ± 101	140 ± 67	0.26 ± 0.12
	CAM5	29 ± 13	57 ± 10	18 ± 12	9 ± 1	306 ± 86	256 ± 119	0.15 ± 0.06
	ModelE2	30 ± 14	61 ± 10	20 ± 7	14 ± 2	405 ± 86	154 ± 72	0.34 ± 0.12

©2014 American Geophysical Union. All rights reserved.

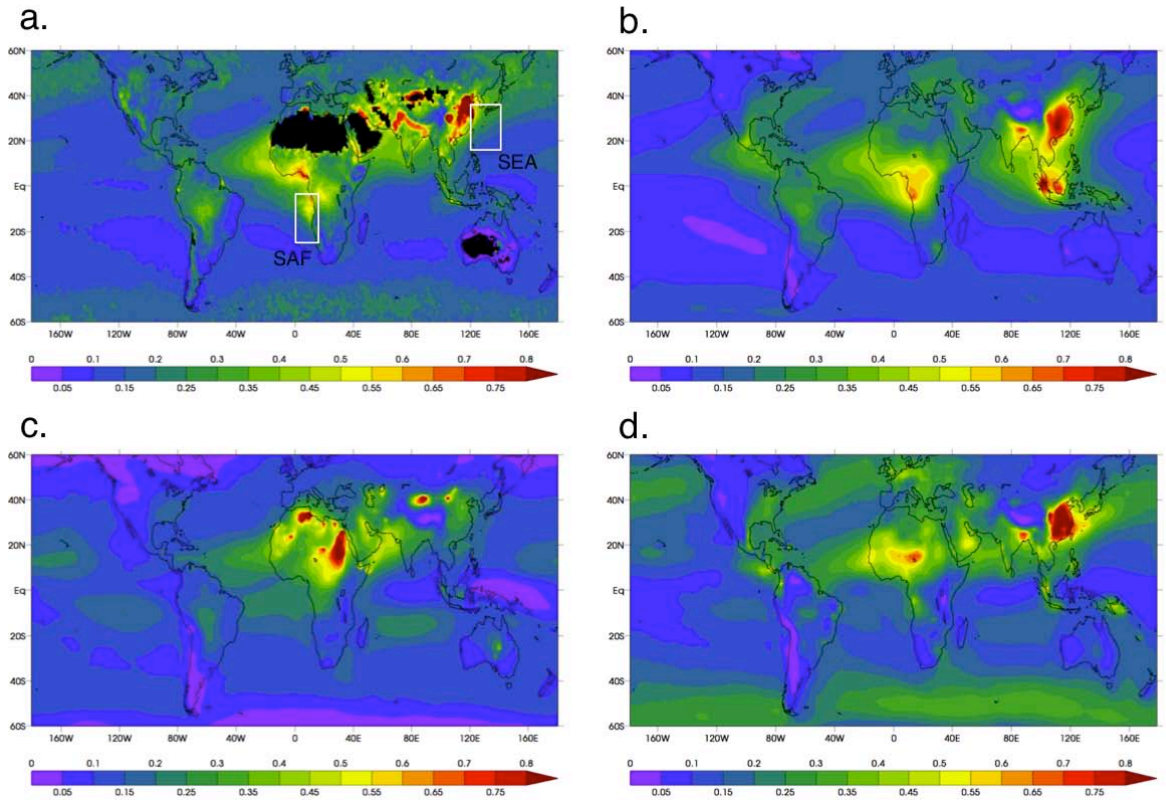

Figure 1. Aerosol optical depth τ_a (unitless) from (a) MODIS observations, (b) AM3, (c) CAM5, and (d) ModelE2. Values are two-year means (2007 – 2008). White outlines represent South African (SAF) and Southeast Asian (SEA) regions.

Accepted

©2014 American Geophysical Union. All rights reserved.

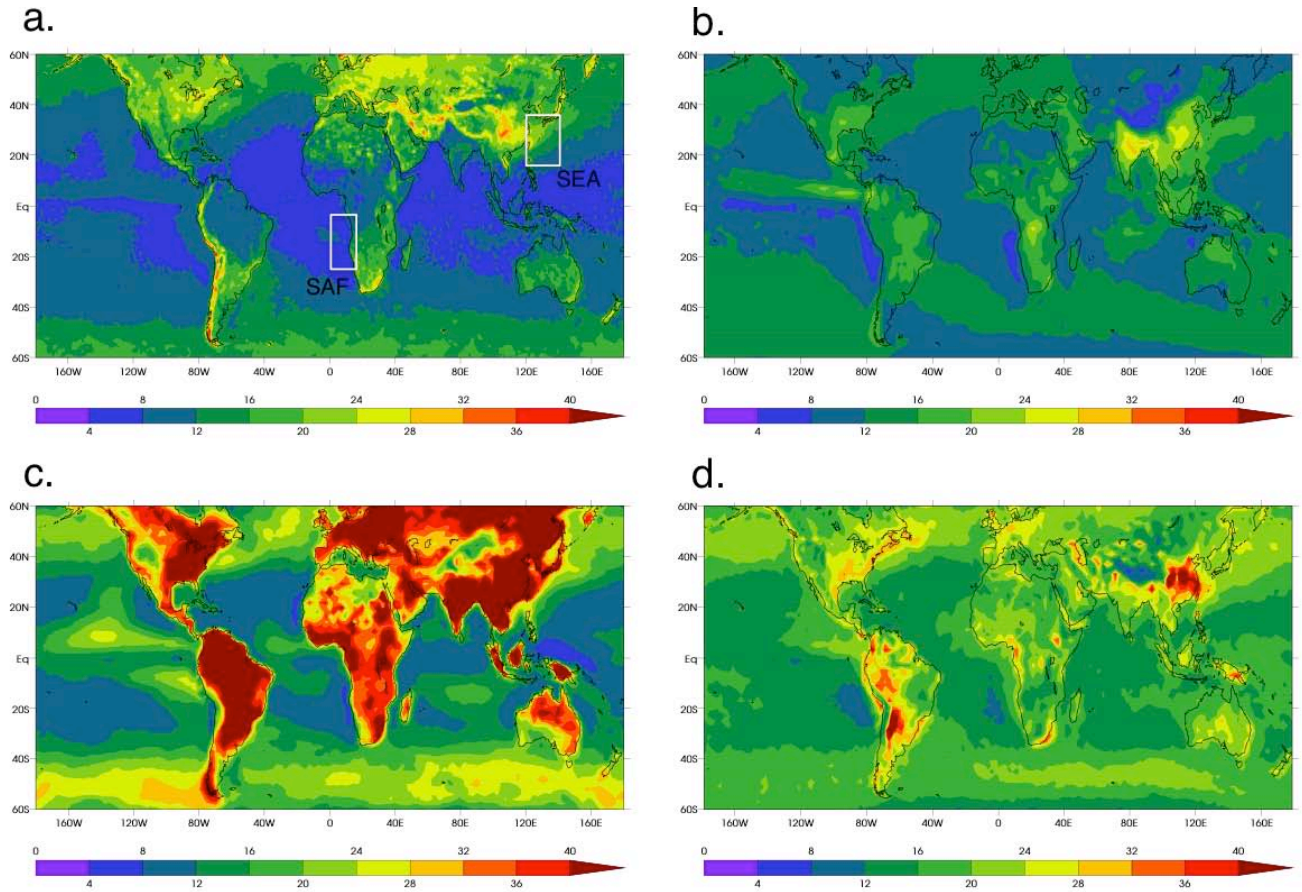

Figure 2. Liquid cloud optical depth τ_c (unitless) from (a) MODIS observations, and satellite-simulated model values from (b) AM3, (c) CAM5, and (d) ModelE2. Two-year means for MODIS observations/simulations (2007 – 2008) are weighted by MODIS observed/simulated liquid cloud fraction [*Pincus et al*., 2012]. Pixels with liquid cloud fraction < 30% are screened. Values are in-cloud concentrations.

Accepted Article

©2014 American Geophysical Union. All rights reserved.

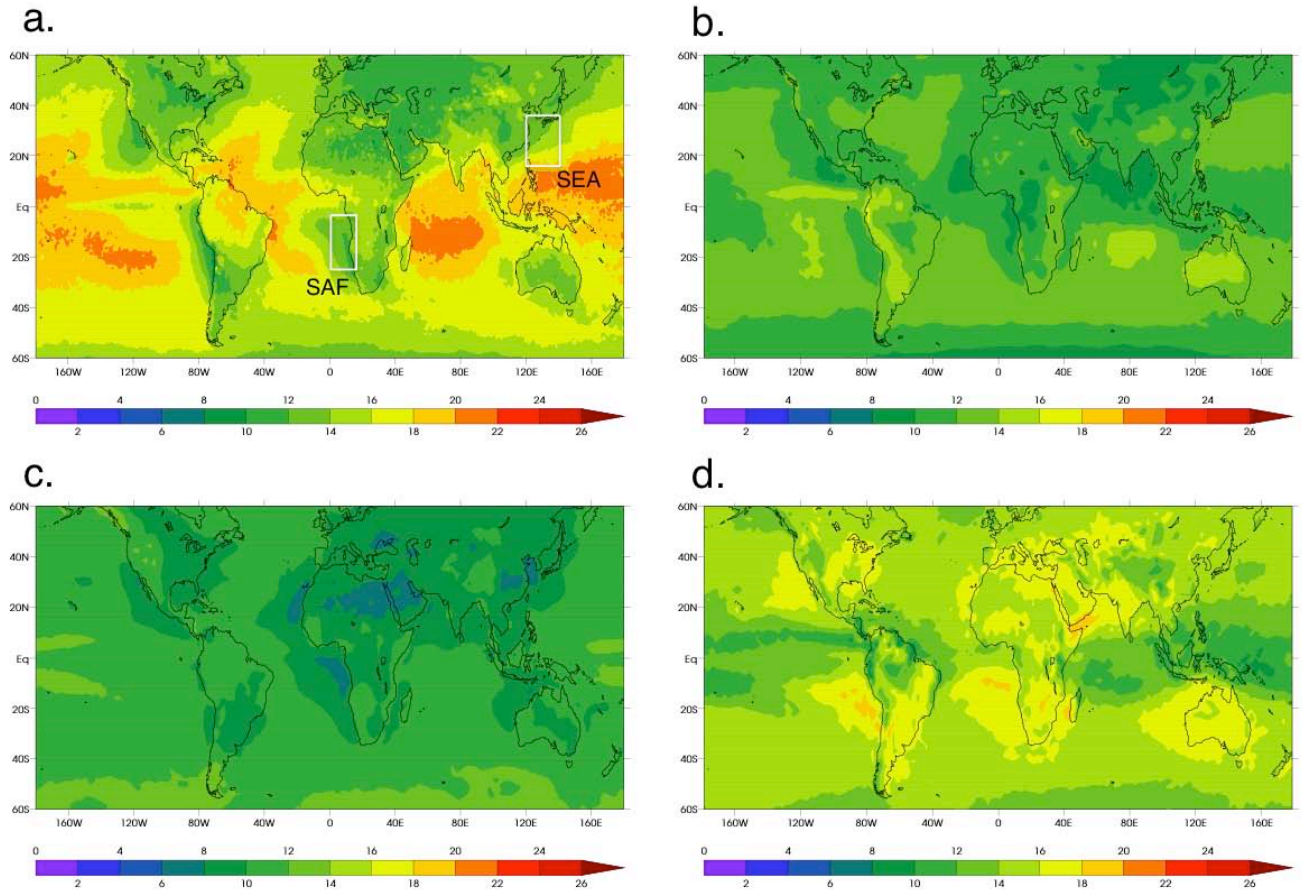

Figure 3. Liquid cloud droplet effective radius r_e (μm) from (a) MODIS observations, and satellite-simulated model values from (b) AM3, (c) CAM5, and (d) ModelE2. See the caption to Figure 2 for more details.

Accepted

©2014 American Geophysical Union. All rights reserved.

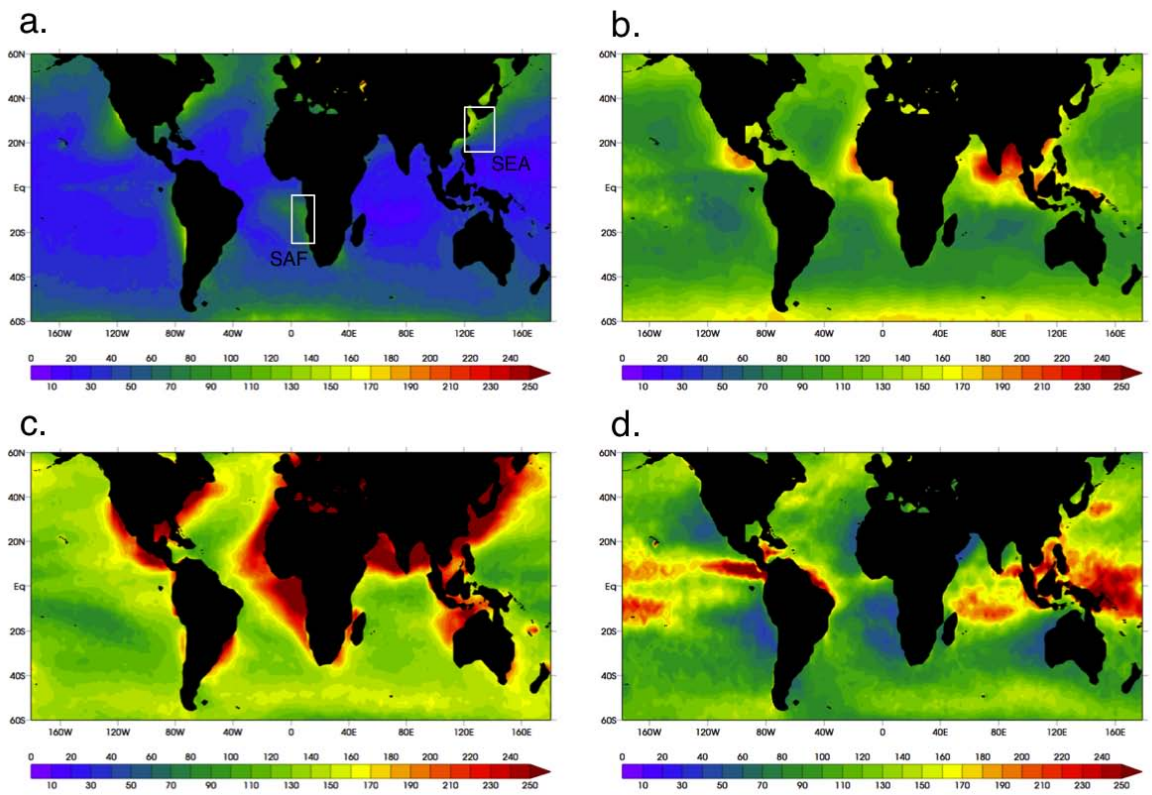

Figure 4. Cloud droplet number concentration N (# cm^{-3}) from (a) MODIS observations, and satellite-simulated model values from (b) AM3, (c) CAM5, and (d) ModelE2. Values are two-year means (2007 – 2008). Observed N is derived using (in-cloud) liquid cloud optical depth τ_c and droplet effective radius r_e via Eq. (5) and (3). Satellite-simulated values of are calculated in the same way using CFMIP Observation Simulator Package (COSP) derived values of τ_c and r_e. Pixels with liquid cloud fraction < 30% are screened. Values are in-cloud concentrations.

Accepted

©2014 American Geophysical Union. All rights reserved.

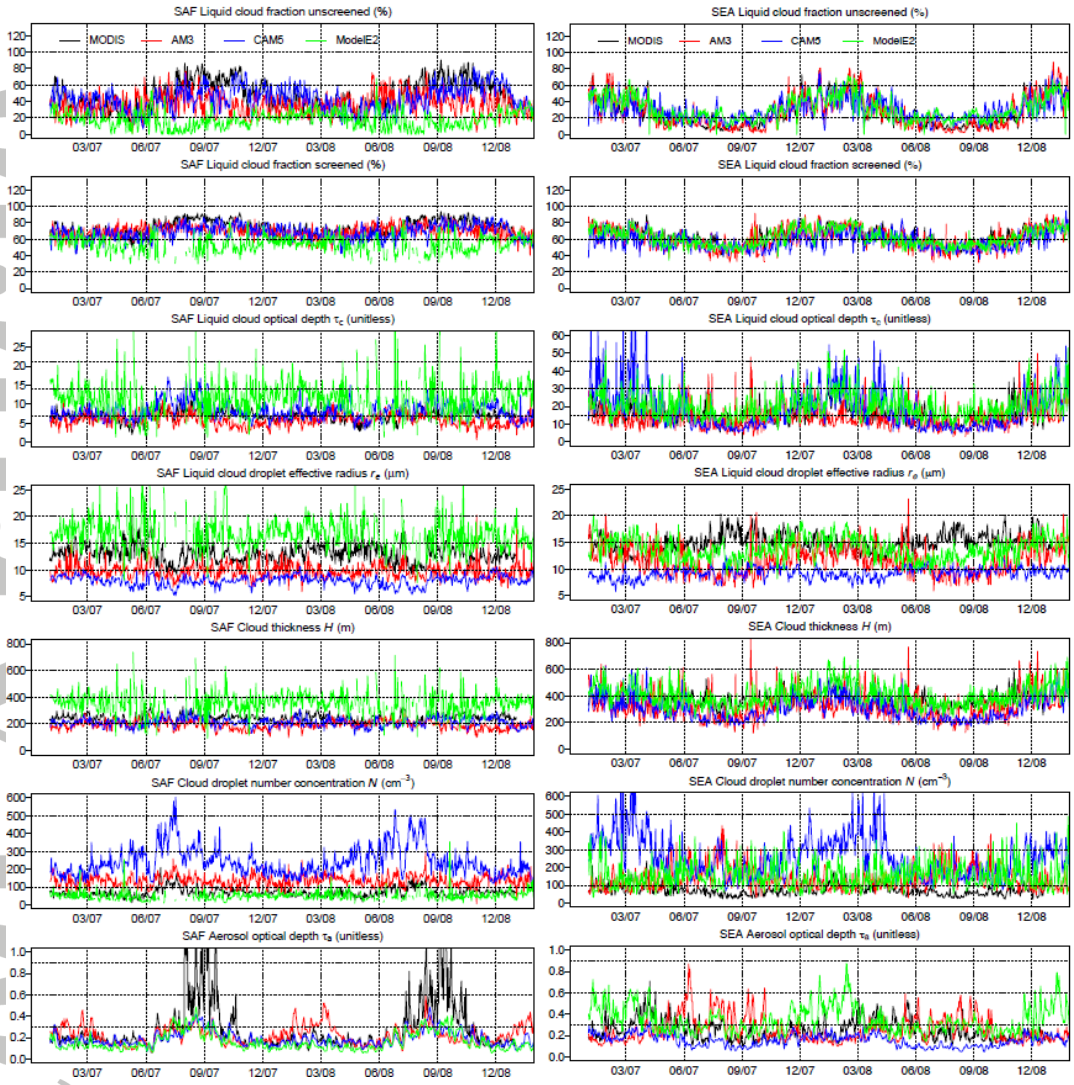

(a) (b)

Figure 5. Spatial mean time series of cloud and aerosol properties from MODIS observations and the three climate models for (a) SAF and (b) SEA. For cloud properties, pixels with liquid cloud fraction < 30% are screened to reduce noise in the retrieval algorithm for *N*. The exception is the top panels in (a) and (b), which show unscreened values for reference. All model values are dailies extracted from the time step corresponding to noon local time in each region, similar to the observed Aqua overpass time of 1330 h local. All modeled cloud properties are satellite-simulated and in-cloud values. *N* was computed using Eq. (5) with both satellite-simulated model values and observations. Corresponding values of cloud thickness *H* were computed using Eq. (4) for both models and observations.

Accepted Article

©2014 American Geophysical Union. All rights reserved.

Accepted Article

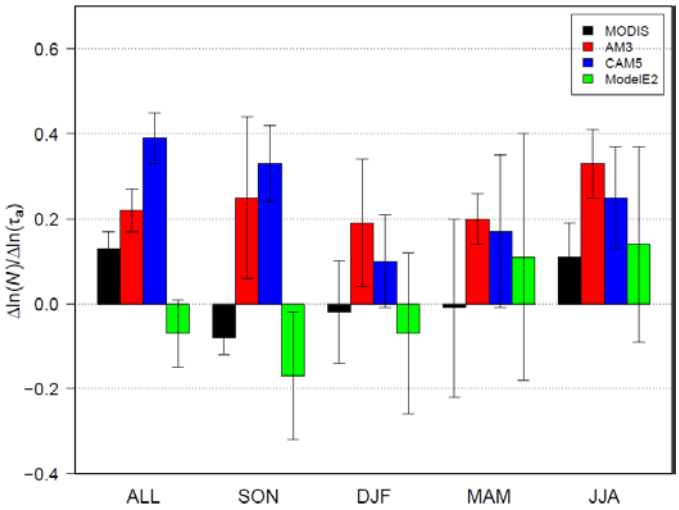

(a)

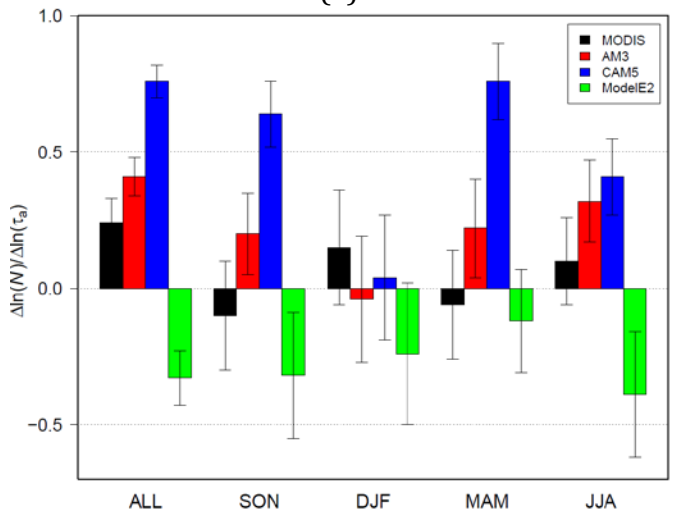

(b)

Figure 6. Total sensitivity of ln(N) to ln(τ_a) for MODIS observations and the three climate models in (a) SAF and (b) SEA. Sensitivities are computed using the time series for N and τ_a shown in Figure 5. See the Figure 5 caption for more details. Sensitivities are shown over for the entire period (January 1, 2007 to January 1, 2009) and individually by season. Numerical values are in the Auxiliary Material. Uncertainty estimates are calculated as 95% confidence interval from daily values.

©2014 American Geophysical Union. All rights reserved.

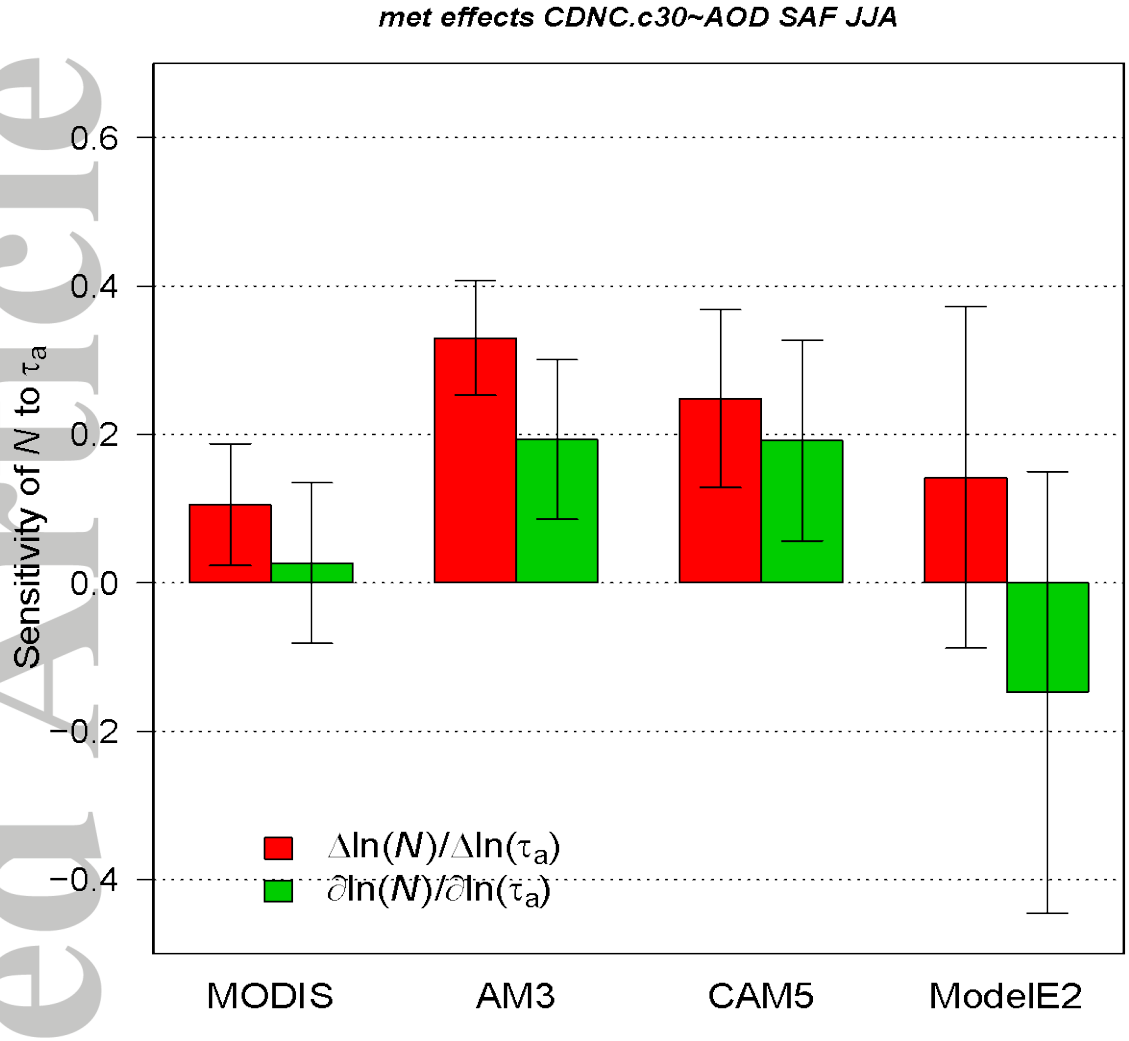

Figure 7. Total (red) and partial (green) sensitivity of ln(N) to ln(τ_a) in SAF during JJA for MODIS observations and the three global climate models. Total sensitivities are identical to those presented in Figure 6. Partial sensitivity removes the confounding influence of relative humidity (in two layers) on N and τ_a. See Section 3.4. Numerical values are in the Auxiliary Material. Uncertainty estimates are calculated as 95% confidence interval using daily values.

Accepted Article

©2014 American Geophysical Union. All rights reserved.

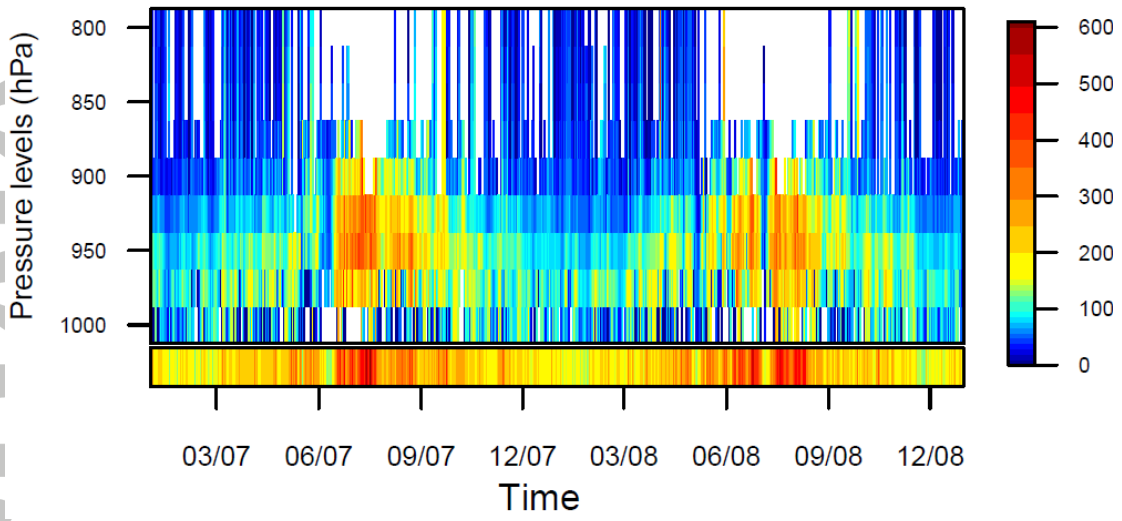

(a)

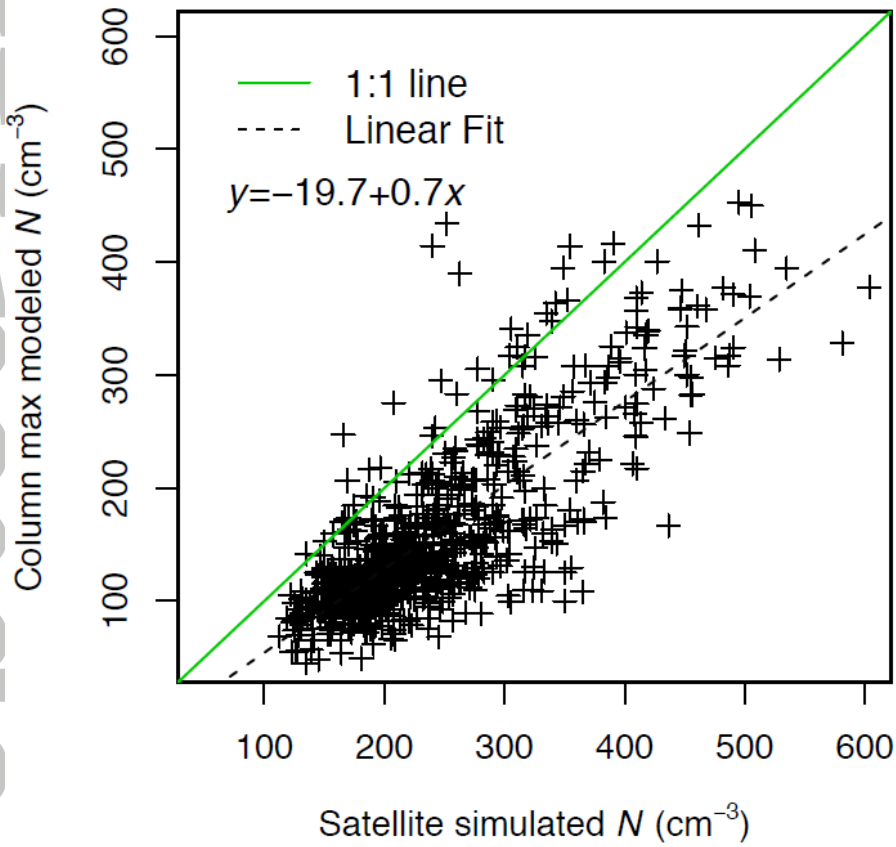

(b)

Figure 8. Comparison of N computed from standard model output versus satellite-simulated values for CAM5. In (a) the curtain plot represents spatial mean vertical profiles of N (cm^{-3}) in SAF computed from standard model output. The color bar below the curtain plot shows satellite-simulated values using the same color scale. (Satellite-simulated values shown here are identical to those shown in Figure 5a.) In (b), column maximum modeled N is shown versus satellite-simulated values (again for CAM5). All values are in-cloud. See Section 4.3 for details on the data screening applied to standard model output. See the Auxiliary Material for other models and regions.

Accepted Article

©2014 American Geophysical Union. All rights reserved.